Structure-function Study of PchB, an Isochorismate-Pyruvate Lyase from *Pseudomonas aeruginosa*

By

Andrew N. Ouellette

Submitted to the Department of Molecular Biosciences and the Faculty of the Graduate School of the University of Kansas in partial fulfillment of the requirements for the degree of Master of Arts in Biochemistry & Biophysics

_____

Chairperson Audrey Lamb

_____

Committee Members Roberto De Guzman

_____

Emily Scott

Date Defended: 06/06/2011

The Thesis Committee for Andrew N. Ouellette

certifies that this is the approved version of the following thesis:

Structure-function Study of PchB, an Isochorismate-Pyruvate Lyase from *Pseudomonas aeruginosa*

_____

Chairperson Audrey Lamb

_____

Committee Members Roberto De Guzman

_____

Emily Scott

Date approved: 06/13/2011

Abstract

Enzymes act as biological catalysts for chemical reactions that would otherwise occur at rates insufficient for the survival and growth of an organism. Understanding the fundamental forces that drive catalysis in enzymes is applicable in the production of novel antibiotics through rational drug design and advancing our understanding of how enzymes achieve incredible rate enhancements over their uncatalyzed reactions. A body of work to understand these forces has been established in the chorismate mutases and the pericyclic reaction they catalyze in the production of prephenate from chorismate.

In *Pseudomonas aeruginosa* a structural homologue of the *Escherichia coli* chorismate mutase EcCM has been found in the isochorismate-pyruvate lyase PchB. While the physiological role of PchB is that of an isochorismate-pyruvate lyase (IPL) in the production of salicylate and pyruvate from isochorismate, PchB also exhibits an adventitious chorismate mutase (CM) activity. The contribution of forces that drive IPL and CM activity in PchB is somewhat controversial with differing hypothesises of transition state stabilization through electrostatic interactions and the formation of a reactive substrate through conformational destabilization. Crystallization and mutational studies have shown the importance of a positive charge at position 42 for efficient catalysis within a dynamic active site loop region of PchB. The charge swap PchB mutant K42E showed no detectable activity and PchB mutant K42A retaining one percent of WT activity.

The WT PchB and PchB mutant K42E crystal structures with the products of the IPL activity (salicylate and pyruvate) bound in the active site show a conserved active site architecture among each other and that of previously solved PchB mutant K42A structure with

salicylate and pyruvate and WT PchB structure with two pyruvate molecules bound in the active site. The conservation of the active site architecture strongly suggests that the differences in the catalytic activities are due to the change in chemical nature of the residue at position 42 within the dynamic active site loop region.

The initial steps into the exploration of the contributions of the dynamic active site loop region to IPL and CM activity in PchB through the current nuclear magnetic resonance spectroscopy assignment of 32 of the 101 backbone resonances of PchB set the foundation for further assignment and collection of relaxation data that will provide loop movement analysis on the picosecond to millisecond time scale.

Acknowledgments

I would like to thank everyone who has helped me throughout the course of my academic career. I would like to thank Qianyi Lou for generating the plasmids for the PchB mutants used in this study and also for the generation of the substrates chorismate and isochorismate which were extensively used throughout the crystallization sparse matrix screening. I would also like to thank Kelli Olechoski for generating the original clone of PchB and also Jingping Lu for the production of the non-his tagged clone of PchB. I would like to acknowledge those that helped in the setup of many PchB crystallization trays: Katie Waugh, Surya Lakhanpal, Allison Ho and Bob Wiggin.

I would also like to thank Roberto De Guzman and Asokan Anbanandam for their help and guidance in setting up and recommendations for specific NMR analysis studies. I would like to extend a special thank you to Fernando Estrada for his patience and guidance during many conversations over the PchB backbone resonance assignments. I would like to acknowledge the resonance assignments previously done on the PchB mutant K42E by Mike Connor and the use of reagents and equipment from the De Guzman lab.

Finally I would like to thank my committee members Audrey Lamb, Roberto De Guzman and Emily Scott for all the advice and guidance they have given me. I would also like to thank Richard Schowen for his many wonderful discussion and lectures over enzyme catalysis and theory and I would like to extend a very special thank you to Audrey Lamb for her support and guidance over the years.

Table of Contents

List of Figures

List of Tables

CHAPTER 1

Enzyme Catalysis in Biological Systems

1.1 Introduction

The Functions of Enzymes

Enzymes function to accelerate chemical reactions within biological systems that otherwise would not occur on a time scale sufficient to support the metabolism of organisms. The upper limit to the rate at which enzymes enhance reaction rates can reach as high as 10^{20}-fold.[1] This is in stark contrast to some uncatalyzed reactions that have half-lives themselves which are billions of years.[2] Over the course of evolution some enzymes have become so efficient at catalysis that their rate constants approach the rate of diffusion of a substrate in solution.[3] In other words every encounter between the substrate and enzyme progresses towards production of products. Not all enzymes achieve this level of efficiency but this serves to highlight the important concept that enzymes are specific for a specific substrate within a biological system. Enzymes can be thought of as vessels that bind specific substrates thereby limiting the substrates interaction with the environment of the solvent while at the same time promoting specific chemical reactions based on the structure and composition of the enzyme's active site. This specificity and efficiency of enzymes supports the massive rate enhancements of chemical reactions and serves to accomplish a host of chemical reactions within biological systems that support the continued metabolism of living organisms.[4]

Enzyme Facilitated Catalysis

Reactions catalyzed by enzymes progress through a series of steps until product formation is complete and released, regenerating the enzyme. First the substrate binds to the active site of the enzyme creating the enzyme substrate complex (ES). The enzyme substrate complex then progresses toward the high energy transition state ([$ES^{‡}$]) through molecular "breathing" motions.[5,6] When the transition state is reached, bonds are broken and formed thereby transitioning the ES complex to the enzyme product complex (EP) which dissociates into free enzyme and product in solution (1).

(1) $$E + S \leftrightarrow ES \leftrightarrow [ES^{‡}] \leftrightarrow EP \leftrightarrow E + P$$

This progression from substrate to product in an enzyme is completely mediated by the binding interactions of the enzyme active site with the substrate.[7]

The Active Site of Enzymes

The enzyme active site is usually a pocketed region of the enzyme where accelerated chemical reactions take place in the presence of bound substrate resulting in the production of products. One way enzyme active sites accomplish massive reaction rate enhancements is by having a surface area composed of various constituent amino acid side chain groups that are able to interact with the substrate through hydrogen bonding, electrostatic interactions and van der Waals forces.[7] Enzymes can also incorporate cofactors such as divalent metal ions (Fe^{2+}, Mg^{2+}, Mn^{2+}, Zn^{2+}) or coenzymes which are metalloorganic or complex organic molecules such as Coenzyme A.[4] This being said, binding of a substrate within the active site of an enzyme alone in a classical "lock and key"[8] sense, where both substrate and enzyme are complimentary to each

other without strain on the substrate, is not sufficient to induce catalysis (Figure 1-1,B). The enzyme must bind the substrate in such a way as to induce strain on the bonds of the substrate thereby supporting the high energy transition state of the chemical reaction over the ground state (E + S) of the substrate free in solution (Figure 1-1,C).[9]

Transition State Theory

Enzymes affect the rate at which a reaction will occur and do not affect reaction equilibria. There is specific activation energy ($\Delta G^{\ddagger}_{cat}$) that must be overcome in the transition state by an ES complex for the reaction to proceed (Figure 1-1,C).[4] The transition state can be described as a high energy, unstable form of the substrate that neither wholly resembles the substrate nor that of the product. The chemical bonds of the transition state molecule are in a quasi-state of simultaneously bond breaking and bond forming. The actual time that a substrate stays in the transition state is very small and has been estimated to be equal to a single bond vibration.[6] The transition state itself represents the highest barrier of free energy that must be crossed for a given substrate molecule to transition to product (Figure 1-1,C).[10] Linus Pauling first popularized Polanyi's idea that for the activation energy to be decreased and a reaction proceed the enzyme must preferentially stabilize the transition state of the substrate and thereby enhance the rate of catalysis.[9] This theory of transition state stabilization is the foundation for drug development that inhibits enzymes by designing transitional state analogues that mimic the transition state of a particular substrate and as a result have a greater affinity for the enzymes active site inhibiting enzyme function.[6]

Figure 1-1. Comparison of reaction mechanisms. Overview of uncatalyzed, "lock and key", and transition state stabilization views of reaction mechanisms. The enzyme is depicted as a blue "pac-man" figure with the substrate depicted as blue and grey balls connected by a blue stick. *Panel A,* Shows the progression of an uncatalyzed reaction showing a large barrier in free energy necessary to produce products. *Panel B,* Shows the classical "lock and key" theory of enzyme catalysis resulting in an even higher free energy barrier than the uncatalyzed reaction. *Panel C,* Shows the theory of transition state stabilization whereas binding lowers the free energy barrier need to cross over to the formation of products. This figured was adapted from Nelson *et al.* 2005.

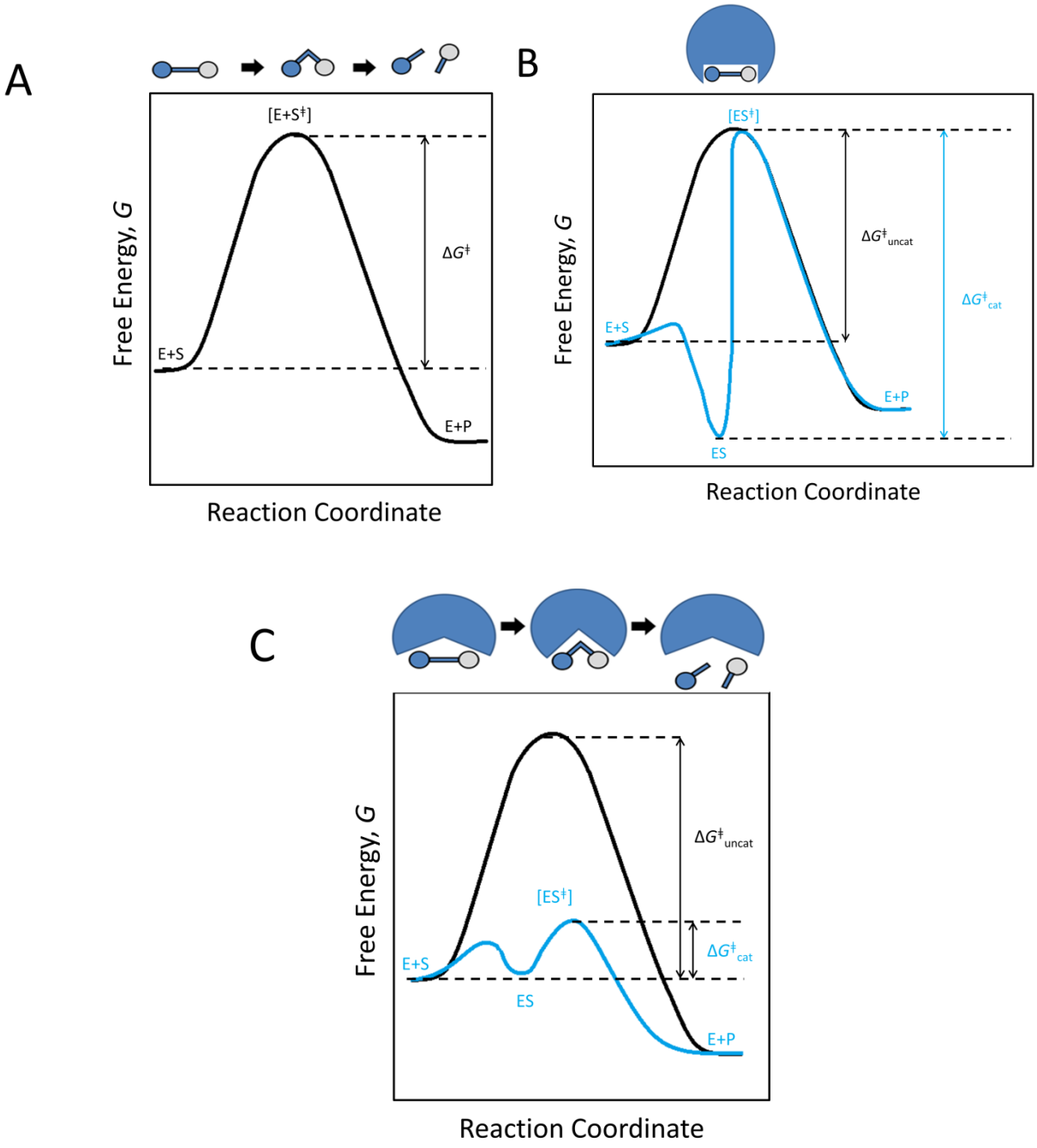

When a substrate binds in the active site of an enzyme it does so through the interactions previously mentioned above (hydrogen bonding, electrostatic interactions and van der Waals forces). These weak interactions are then optimized in the transition state. The weak interactions in the initial binding event in the active site of an enzyme serve multiple purposes in bringing the substrate closer to the transition along the reaction coordinate. This includes decreasing the entropy of the substrate by aligning reactive groups into high energy conformations thereby lowering the freedom of the molecule.[11] This preorganization of the substrate alone has been shown to have rate enhancements of $10^{8.4}$ Also as the substrate binds, the solvation shell of water molecules that stabilize the substrate in solution are lost and hydrogen bonding is replaced by functional groups within the active site resulting in what is called an "induced fit" (Figure 1-1,C). This induced fit of the enzyme substrate complex brought on by binding of the substrate results in a conformation change in the enzyme that aligns the reactive groups in the active site necessary for catalysis and optimizes their interaction with the substrate.[12] While binding interactions account for a majority of rate enhancement for an enzyme[9,13] the specific interactions of the aligned reactive groups contribute to the catalytic mechanism through three main mechanisms: general acid base catalysis, covalent catalysis and metal ion catalysis.[4,14]

General Acid-Base Catalysis

The transfer of protons (H^+) to and from a substrate intermediate in an enzyme's active site helps direct the substrate intermediate towards the transition state and rate enhancements over the uncatalyzed reaction on the order of 10^2 to 10^5 are observed.[4] When catalysis is dependent on H^+ (H_3O^+) or OH^- ions from water alone within the active site it is referred to as

specific acid-base catalysis. The term general acid-base catalysis describes the transfer of protons mediated by a Brønsted acid (species that can donate a proton) or Brønsted base (species that can accept a proton), these include many of the amino acids such as lysine, arginine, cysteine, histidine, serine, tyrosine and glutamic and aspartic acid.[4,14] Many times enzymes incorporate both general acids and bases within their reaction mechanisms or in what is known as a concerted general acid-base mechanism. General acid-base catalysis is the most common form catalysis in biological systems.[4,13,14]

Covalent Catalysis

The enzymatic mechanism utilizing covalent catalysis is a stepwise mechanism that first involves a transient intermediate form of the substrate covalently bonded to the enzyme. This interaction lowers the free energy of activation and aligns reactive groups bringing the substrate closer to the transition state. This creates a step wise reaction mechanism that is subsequently dependent on the breakdown of the covalent bonded transient intermediate to produce to products and to regenerate free enzyme. The mechanism of covalent catalysis proceeds through nucelophilic and electrophilic processes.[14] All of amino acids mentioned above for general acid-base catalysis are capable of interacting with substrate as nucleophiles, generating the formation of covalent bonds with the substrate.[4] The catalyzed reaction proceeds through an initial nucleophilic attack on the substrate that generates a covalent bond between the now transient intermediate and enzyme and produces an unstable charged group within the intermediate. The electrons from the charged intermediate can be/are then shuttled to a now electrophilic group within the enzyme. To eliminate the covalently bound product and regenerate the enzyme, a

nucelophilic attack must occur between the covalently bound intermediate and enzyme resulting in again a charged intermediate that then breaks down and shuttles electrons to an electrophile within the enzyme thereby breaking the covalent bond and releasing the product. Many proteases such as chymotrypsin use covalent catalysis to carry out their reaction mechanisms.[4,14,15]

Metal Ion Catalysis

The weak interactions found within the active site of an enzyme can include divalent metal ions (Fe^{2+}, Mg^{2+}, Mn^{2+}, Zn^{2+}) tightly bound to enzymes active site or other ions that come directly from solution itself (Na^{+}, K^{+}, Mg^{2+}, Ca^{2+}). Metal ions are required for catalysis in a third of all known enzymes.[4,14] The use of metal ions help to move the substrate towards the transition state by a number of mechanisms. A metal ion can provide charge stabilization for the transition state by acting as a Lewis acid. The major advantage of metal ions in this regard is that metal ion concentration is independent of the pH, meaning that there can be high levels of metal ions available for catalysis, independent of the concentration of hydrogen ions available in solution. A metal ion can generate OH^{-} ions by effecting bound water molecules promoting nucelophilic catalysis. The position of metal ions with the active site themselves can also lead to charge shielding of certain chemical groups within the substrate, negating repulsion effects that would otherwise inhibit further binding of the substrate or enhance selective charges formed during the transition state.[14]

Proximity and Orientation Effects

All of the above interactions serve to lower the activation energy of catalysis by preferentially binding the transition state of a substrate over that of the ground level energy conformation. The various methods incorporated thereafter (general acid-base, covalent and metal ion catalysis) account for a relatively small portion of lowering the activation energy relative to the initial binding of the substrate.[4,9,14] It is important to note that the reaction mechanisms incorporated by enzymes mimic those used in uncatalyzed reactions through what are referred to as proximity and orientation effects. This is to say that the reactive groups must come within the proper distance and alignment to allow catalysis to proceed. This preordering of the substrate into a high energy conformation through alignment and positioning of the reactive groups allow for a substantial decrease in the activation energy needed to achieve catalysis.[9,14] In this way proximity and orientation effects can be thought of as supporting a reactive substrate conformation.

Pericyclic Reactions

If the alignment and orientation of reactive groups is a driving force towards the transition state in a multi-substrate reaction then one could hypothesize that within a single substrate reaction these intramolecular forces would be an even greater driving force along the reaction coordinate. In essence enzymes use proximity and orientation effects to create a subpopulation of reactive substrate conformations higher in energy than a ground state experienced in solution. This leads to the transition state thereby enhancing the rate of catalysis over the uncatalyzed reaction.[9] This idea of producing a reactive substrate conformation and the

resultant rate enhancement is apparent in pericyclic reactions, which are seldom found in biology.[16] Pericyclic are concerted reactions that have a cyclic transition state where bond breaking and formation is dependent on interacting orbitals within the cyclic intermediate.[17] The ordering of the substrate into a reactive substrate conformation is sufficient to lead to catalysis.[18] Enzymes that catalyze these reactions do not utilize general acid-base, covalent or metal ion catalytic mechanisms. Understanding pericyclic reactions has become a major area of interest in the field of enzymology because pericyclic reactions represent a window into understanding the fundamental forces that drive catalysis.

Work done on enzymes that catalyze pericyclic reactions has led to the introduction of the term "NAC" from *in silico* findings from Bruce and co-workers.[18] The NAC stands for Near Attack Conformation and refers to a required conformation of the substrate in which the reactive groups are aligned for the reaction. The NAC has been proposed to be considered a ground state because the aligned reactive groups neither participate in bond breaking or bond formation while in the state of a NAC and therefore the NAC is not equivalent to the transition state.[18] While the idea of the NAC as a true ground state is debatable[1] the idea of what a NAC represents is not hard to envision and provides a viewpoint into what is required of enzymes that catalyze pericyclic reactions.

Selective Binding of the Transition State by Enzymes

We have already discussed how the ability of an enzyme to catalyze a reaction is dependent on the ability of the enzyme to bind the transition state. What was not discussed before is how the rate of enhancement for a catalytic enzyme is proportional to the affinity of the

enzyme for the transition state as shown below (3). This is under the assumption that the chemical step is the rate limiting with eq 1,2 and 3 representing a single substrate system.[19] Equation 1 shows

(1)
$$\begin{array}{ccccc} & & K_{UN}^{\ddagger} & & \\ E+S & \leftrightarrow & E+S^{\ddagger} & \rightarrow & E+P \\ K_S \updownarrow & & K_{CAT}^{\ddagger} & \updownarrow K_{TS} & \\ ES & \leftrightarrow & ES^{\ddagger} & \rightarrow & E+P \end{array}$$

(2)
$$\frac{K_{TS}}{K_{UN}^{\ddagger}} = \frac{K_S}{K_{CAT}^{\ddagger}}$$

(3)
$$K_{TS} = \frac{K_{UN}^{\ddagger}}{K_{CAT}^{\ddagger}} K_S$$

the thermodynamic relationship between binding of the ground state and transition state for an enzyme and single substrate. This leads to the relative comparison of the dissociation constants (K_S,K_{TS}) with the uncatalyzed ($K_{UN}^{\ddagger}$) and catalyzed ($K_{CAT}^{\ddagger}$) pseudo equilibrium constants (2). Rearrangement of eq 2 results in eq 3, showing that the dissociation constant (K_{TS}) of the enzyme transition state complex ($ES^{\ddagger}$) is equal to the relative rate enhancement of the enzyme ($K_{UN}^{\ddagger}$/ $K_{CAT}^{\ddagger}$) multiplied by the dissociation constant (K_S) of the enzyme substrate complex (ES). If the affinity for the transition state is directly proportional to the rate enhancement then the greater the rate at which an enzyme enhances a reaction should be evident by that enzyme's ability to bind the transition state of the substrate.[19] The catalytic power of enzymes is therefore contingent upon the interactions the enzyme makes with the substrate that correlate to binding of the transition state and the dynamic forces that drive these interactions.

This thesis focuses on understanding the structural and dynamic forces that add in the pericyclic reactions catalyzed by PchB, an isochorismate pyruvate-lyase from *Pseudomonas aeruginosa* with adventitious chorismate mutase activity. Protein X-ray crystallography and nuclear magnetic resonance studies were carried out to ascertain the contributions of charge stabilization and loop dynamics to the efficiency of PchB's activity. The goal of this work is to provide structural and dynamic information that can be used to enhance our understanding of the fundamental concepts of enzyme catalysis and contribute to the future development of novel inhibitors against PchB.

The work presented within would not be possible without previous structural and mechanistic studies of PchB. Here we review the major contributions of our group that began to elucidate the fundamental forces that drive catalysis in PchB.

1.2 PchB

Physiological Role of PchB

The physiological role of PchB in *Pseudomonas aeruginosa* is that of an isochorismate pyruvate-lyase catalyzing the production of salicylate and pyruvate from isochorismate.[20] The salicylate is then ultimately incorporated into the siderophore pyochelin. Siderophores are low molecular weight iron chelators that serve as bacterial virulence factors.[21] Pyochelin scavenges iron from the bacterial host allowing for the continued colonization and growth of *P. aeruginosa*.

Initial Structural Studies of PchB

Originally structural studies were carried out on WT PchB yielding two crystal structures of PchB, apo (PDB code: 2H9C) and pyruvate (PDB code: 2H9D) bound structures.[22] The

crystal structures showed that PchB is a structural homologue of the *Escherichia coli* chorismate mutase EcCM consisting of an intertwined dimer (Figure 1-2). Major findings of the first PchB crystallization study included that the active site loop becomes ordered in the presence of two pyruvate molecules bound in the active site with five of the nine side chain interactions in the active site of EcCM conserved among PchB.[22] This reduction in side chain interactions within the active site of PchB, relative to EcCM, likely serves as the basis for the catalytic promiscuity of PchB as an isochorismate-pyruvate lyase (IPL) and chorismate mutase (CM).[22] This work established the foundation for further structural and mechanistic studies.

Mutational Studies of PchB

In the second published study from our group a variety of PchB mutants were made at K42, A43 and I87.[23] These mutations served to test various aspects of the proposed mechanism of PchB's catalytic activity. Mutations of residue K42 included K42A, K42E, K42Q and K42H. These mutations addressed the ability of K42 to stabilize the transition state through electrostatic interactions. The alanine mutation provided the absence of any charge at position 42 while the glutamic acid mutation provided a negative charge relative to the WT positive charge found with lysine. The K42Q mutation produced a polar uncharged side chain while the K42H mutation allowed for a titratable positive charge based on the pH of the solution. The A43P mutation was introduced to slow down the active site loop dynamics by inserting a rigid proline into the flexible loop region. The I87T variant was based on a previous reported study that resulted in a PchB mutant that exhibited CM activity but lacked IPL activity.[20,23]

Circular Dichroism Spectroscopy

The original mutation studies performed on EcCM resulted in a lack of activity were hypothesized to have disrupted the active site architecture. This is supported by an altered

circular dichroism (CD) spectrum peak at ~210 nm not consistent with the all alpha helical structure of WT EcCM (Figure 1-2).[23,24] Circular dichroism spectroscopy was performed on PchB mutants to assay for changes in the overall secondary structure of PchB. All of the mutations produced in PchB to date which have resulted in CD spectra similar to WT PchB with local minima at ~210 and ~225 nm supporting that the secondary helical structure had been preserved among all PchB mutants.[25,26]

IPL and CM activity

IPL and CM activity assays were performed for all WT PchB and mutants. The results showed a sharp decrease in the efficiency (k_{cat}/K_m) of PchB IPL and CM activity among several mutants. Most notable was the 100-fold decrease in IPL activity exhibited by the non-charged K42A mutant, no detectable activity for the charge swap mutant K42E and a titratable activity found for the K42H mutant (Table 1-1).[21] While the CD spectroscopy showed no overall change in the secondary structure of PchB, the IPL and CM activity assays show that the mutations have altered PchB's ability to perform catalysis, likely as a result of by changes in PchB's active site architecture. The A43P mutation introduced to slow the dynamics of the active site loop was the closest to WT PchB activity retaining 72% and 86% of wild type activity for CM and IPL activity respectively.

Crystal Structures

The crystal structures of the PchB mutant K42A with salicylate and pyruvate bound and apo PchB mutant I87T were determined in the second published of PchB from our group. While the I87T structure showed a greater degree of flexibility with an overall increased disorder in the active site loop region relative to the apo WT PchB structure. The I87T mutant has increased disorder extending ~5 amino acids on either side of the active site loop relative to the disorder

Figure 1-2. Secondary structure of PchB and EcCM. Global view of secondary structure of WT PchB and EcCM. *Panel A*, Cartoon representation of intertwined dimmer of WT PchB with two molecules of pyruvate bound (green sticks, PBD code: 2H9C). *Panel B*, Cartoon representation of intertwined dimer of EcCM with the transition state analog, bicyclo dicarboxylic acid, bound (PBD code: 1ECM). PchB and EcCM are structural homologues.

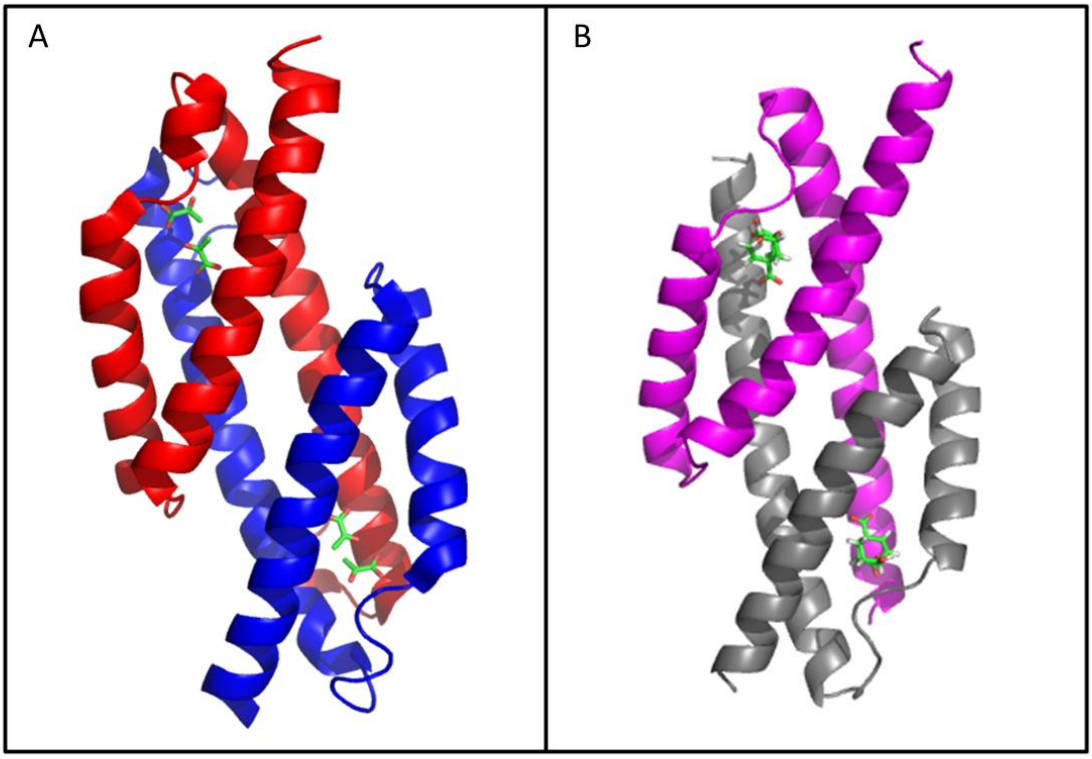

Table 1-1. WT PchB and selected mutant steady state kinetic parameters. Table showing changes in IPL activity for WT PchB and mutants K42A, K42E and K42H (pH of 7.5). Notice the two orders of magnitude decrease in catalytic efficiency (k_{cat}/K_m) between WT PchB and mutant K42A and also between K42A and K42E. Figured adapted from Luo *et al.* 2009.

Side Chain		K_m (μM)	k_{cat} ($x10^{-3}$ s^{-1})	k_{cat} / K_m ($M^{-1}s^{-1}$)	% WT (k_{cat} / K_m)
+	WT	4.3±0.2	177±2.0	41100	-
	K42A	51±3.0	24.5±0.5	480	1
--	K42E	*	*	-	-
titratiable	K42H**	57±2.0	37.0±0.7	650	2
	A43P	5.3±0.1	188±5.0	35500	86

* = below the limits of detection (0.3pmol for IPL assay) **= pH 7.5

found in the apo WT PchB structure.[21] Most notable was the PchB mutant K42A with the products of PchB's IPL activity bound in the active site. The structure was found to be comparable to that of WT PchB with two pyruvate molecules bound in the active site and that of the wrong-ligand[20] model of WT PchB with salicylate and pyruvate bound in the active site. The active site architecture of K42A was shown to coordinate the carboxylic groups of salicylate and pyruvate through two arginines (R14 & R31, Figure 1-3).

Elucidating the Mechanism of PchB Activity

The initial mechanistic and structural studies of PchB provided the basis of the work undertaken for this thesis which is focused on addressing two major questions: 1) is the active site architecture conserved among all WT PchB and mutants, specifically in regards to K42E where no detectable activity was determined and 2) how much do the active site loop dynamics contribute to catalysis? The prior production of apo WT PchB and salicylate and pyruvate bound K42A structure provides a standard to compare all further structures of PchB. The PchB activity assays provide the groundwork towards understanding what is essential in supporting the transition state for PchB activity and set the direction for further exploration.

Figure 1-3. Active site overlay of WT PchB and mutant K42A crystal structures. WT PchB with 2 pyruvate molecules bound (green and light green sticks, PDB Code: 2H9D). PchB mutant K42A with salicylate and pyruvate bound (magenta and dark pink sticks, PDB Code: 3HGX). Arginine 31 and arginine 14 are shown to align the carboxylates of salicylate and pyruvate in 3HGX and the two pyruvate molecules in 2H9D. The overall active site architecture and positioning of salicylate and pyruvate remain consistent in both WT PchB and K42A mutant structures. Amino acids are labeled as PchB numbering

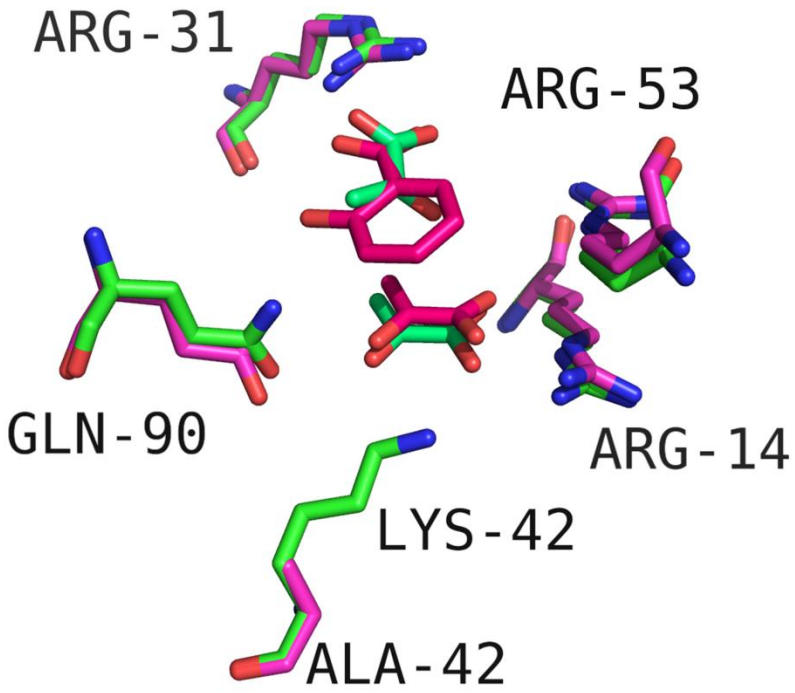

References

1. Borman, S. Much ado about enzyme mechanisms. *C&E News* **88**, 35-39 (2004).
2. Wolfenden, R. & Snider, M.J. The depth of chemical time and the power of enzymes as catalysts. *Acc Chem Res* **34**, 938-945 (2001).
3. Alberty, R., Hammes, G., Application of the Theory of Diffusion-Controlled Reactions to Enzyme Kinetics. *J Phys Chem* **62**, 154-162 (1958).
4. Nelson, D.L. & Cox, M.M. Lehninger Principles of Biochemistry (2005).
5. Karplus, M. Molecular dynamics simulations of biomolecules. *Acc Chem Res* **35**, 321-323 (2002).
6. Schramm, V.L. Enzymatic transition states and transition state analog design. *Annu Rev Biochem* **67**, 693-720 (1998).
7. Warshel, A. et al. Electrostatic basis for enzyme catalysis. *Chem Rev* **106**, 3210-3235 (2006).
8. Fisher, E. Einfluss der Configuration auf die Wirkung der Enzyme. *Ber Dt Chem Ges* **27**: 2985–2993 (1894).
9. Pauling, L. Nature of forces between large molecules of biological interest. *Nature* **161**, 707-709 (1948).
10. Benkovic,S., Hammes, G., Hammes-Schiffer, S., Free-Energy Landscape of Enzyme Catalysis. *Biochemistry* **47**, 3317-3321 (2008).
11. Cannon, W.R. & Benkovic, S.J. Solvation, reorganization energy, and biological catalysis. *J Biol Chem* **273**, 26257-26260 (1998).
12. Koshland, D. Application of a theory of enzyme specificity to protein synthesis. *Proc Natl Acad Sci U S A* **44**, 98-104 (1958).
13. Jencks, W.P. Mechanism of Enzyme Action. *Annu Rev Biochem* **32**, 639-676 (1963).
14. Voet, D. & Voet, J.G. Biochemistry (Wiley, 2004).
15. Blow, D. Structure and mechanism of Chymotrypsin. *Acc Chem Res* **9**, 145-152 (1976).
16. DeClue, M. S., Baldridge, K. K., Kunzler, D. E., Kast, P. and Hilvert, DIsochorismate Pyruvate Lyase: A Pericyclic Reaction Mechanism? *J Am Chem Soc* **127**, 15002– 15003 (2005).
17. Wade, L. Organic Chemistry (Pearson Prentice Hall, 2006).
18. Bruice, T.C. & Lightstone, F.C. Ground state and transition state contributions to the rates of intramolecular and enzymatic reactions. *Acc Chem Res* **32**, 127-136 (1999).
19. Mader, M.M. & Bartlett, P.A. Binding Energy and Catalysis: The Implications for Transition-State Analogs and Catalytic Antibodies. *Chem Rev* **97**, 1281-1302 (1997).
20. Gaille, C., Kast, P. & Haas, D. Salicylate biosynthesis in Pseudomonas aeruginosa. Purification and characterization of PchB, a novel bifunctional enzyme displaying isochorismate pyruvate-lyase and chorismate mutase activities. *J Biol Chem* **277**, 21768-21775 (2002).
21. Lamont, I.L., Beare, P.A., Ochsner, U., Vasil, A.I. & Vasil, M.L. Siderophoremediated signaling regulates virulence factor production in *Pseudomonas aeruginosa*. *Proc Natl Acad Sci U S A* **99**, 7072-7 (2002).
22. Zaitseva, J., Lu, J., Olechoski, K.L. & Lamb, A.L. Two crystal structures of the isochorismate pyruvate lyase from Pseudomonas aeruginosa. *J Biol Chem* **281**, 33441-33449 (2006).
23. Qianyi, L., Olucha, J. & Lamb, A.L. Structure-Function Analyses of Isochorismate-Pyruvate Lyase from *Pseudomonas aeruginosa* Suggest Differeing Catalytic Mechanisms

for the Two Pericyclic Reactions of This Bifunctional Enzyme. *Biochemistry* **48**, 5239-5245 (2009).

24. Liu, D.R., Cload, S.T., Pastor, R.M. & Schultz, P.G. Analysis of active site residues in *Escherichia coli* chorismate mutase by site-directed mutagenesis. *J Am Chem Soc* **118**, 1789-1790 (1996).
25. Hur, S. and Bruice, T. C. The mechanism of catalysis of the chorismate to prephenate reaction by the *Escherichia coli* mutase enzyme *Proc Natl Acad Sci U S A* **99**, 1176-1181 (2002).
26. Hur, S. and Bruice, T. C. The near attack conformation approach to the study of the chorismate to prephenate reaction *Proc Natl Acad Sci U S A* **100**, 12015- 12020 (2003).

CHAPTER 2

Protein X-ray Crystallography of PchB, an Isochorismate-Pyruvate Lyase from *Pseudomonas aeruginosa*

The work within has been submitted to *Biochemistry*. "pH Dependence of Catalysis by *Pseudomonas aeruginosa* Isochorismate-Pyruvate Lyase: Implications for Transition State Stabilization and the Role of Lysine 42"
Jose Olucha, Andrew N. Ouellette, Qianyi Luo, and Audrey L. Lamb

2.1 Introduction

PchB, an Isochorismate-Pyruvate Lyase from *Pseudomonas aeruginosa*

PchB is a bi-functional enzyme of *Pseudomonas aeruginosa* that exhibits a physiological isochorismate pyruvate lyase (IPL) activity and an adventitious chorismate mutase (CM) activity.[1] PchB's physiological IPL activity catalyzes the formation of salicylate from isochorismate in conjunction with the production of isochorismate from chorismate facilitated by PchA (Figure 2-1, A).[2] Specifically, the conversion of isochorismate to salicylate and pyruvate by PchB is catalyzed through a (1,5)- pericyclic hydrogen transfer mechanism.[3] The C2 hydrogen is transferred to C9 of the enolpyruvate tail of isochorismate which promotes the breaking of the ether bond between C3 and O7 resulting in the release of the enolpyruvate tail as pyruvate and the formation of salicylate from isochorismate (Figure 2-1, B). PchB's adventitious CM activity catalyzes the formation of prephenate from chorismate (Figure 2-1, C).[1] The production of prephenate proceeds through a (3,3)-sigmatropic pericyclic rearrangement.[4]

Figure 2-1. Overview of reactions catalyzed by PchA and PchB. *Panel A*, Overview of the production salicylate and pyruvate from chorismate facilitated by PchA and PchB. *Panel B*, Reaction mechanism of PchB's IPL activity through a (1,5)- pericyclic hydrogen transfer mechanism. *Panel C*, Reaction mechanism of PchB's CM activity through a (3,3)- pericyclic rearrangement.

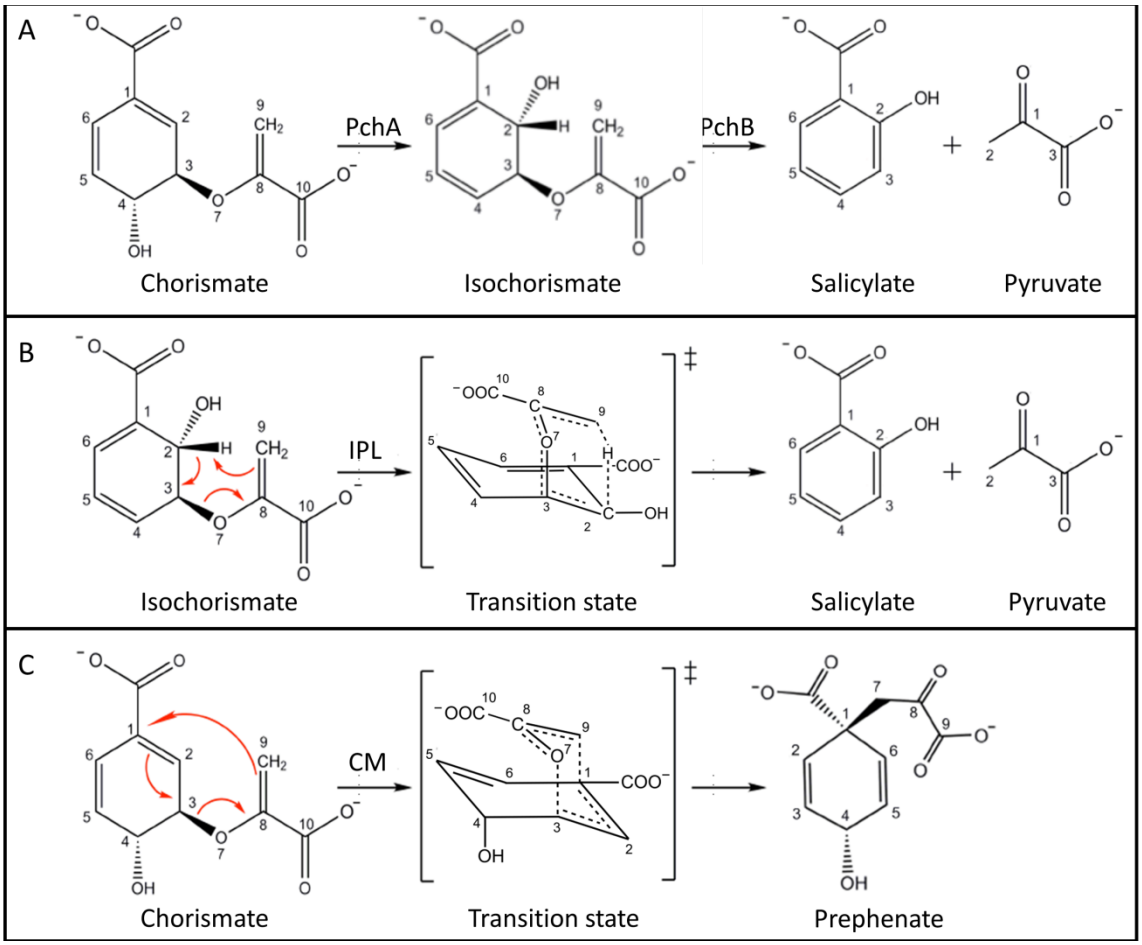

The reaction results in a concerted but asynchronous bond breaking of the ether bond between C3 and O7 and bond making between C1 and C9 of the enolpyruvate tail (Figure 2-1, C).

The rate of PchB's IPL activity is ~$4x10^4$ $M^{-1}s^{-1}$ while the rate of PchB's CM activity is considerably lower at ~$1x10^2$ $M^{-1}s^{-1}$.[5] PchB shares no sequence identity with other salicylate synthases but is a structural homologue of the CM from *Esherichia coli* (EcCM) with 20% sequence identity.[6]

Previous comparisons of the active site of EcCM and PchB show only 5 of the 8 residues important for CM activity in EcCM to be conserved in PchB.[5,6] This serves as one explanation of how PchB can catalyze two different reactions within one active site. What both the CM and IPL activities of PchB do have in common though is the incorporation of a pericyclic transition state (Figure 2-1, B & C).[3,4] Pericyclic reactions are unusual in nature and have been extensively studied in chorismate mutases.[7-10] CM activity and hence pericyclic reactions pose a unique model for studying the fundamental forces that drive enzymes catalysis. This is because pericyclic reactions do not follow the traditional norms of enzyme catalysis as they do not require general acid/base, have no covalent intermediates or depend on metal ions to catalyze the formation of products. The question then becomes how do enzymes that catalyze pericyclic reactions accomplish rate enhancement relative to the uncatalyzed reaction?

Currently in the field of enzymology there are two schools of thought as to how enzymes catalyze pericyclic reactions, specifically for the chorismate mutases. The first involves stabilization of the transition state through electrostatic interactions that balance the developing negative charges formed as the substrate transitions to product.[11,12] This has been supported in crystal structure analysis of both EcCM and the *Bacillus subtilis* CM BsCM with the transition state analog (TSA) oxabicyclic acid bound in the active site along with the recent crystal

structure of PchB mutant K42A with salicylate and pyruvate bound in the active site (Figure 2-2).[5,13] Analysis of the active sites of the three chorismate mutases show electrostatic interactions that would support a developing negative charge on the ether oxygen in the case of the TSA . Hydrogen bonding interactions orient the carboxylic groups of TSA molecules in BsCM and EcCM and the carboxylic groups of salicylate and pyruvate in PchB mutant K42A into a pseudo-diaxial conformation resembling the transition state for CM activity.[5,7,9,13,14] Further evidence of supportive electrostatic interactions can be found in mutagenesis studies of BsCM, EcCM and PchB. Mutations disrupting the equivalent positive charge at arginine 90 in BsCM or lysine 39 in EcCM or lysine 42 in PchB (K42A) led to a complete lack of CM activity in the case of BsCM and EcCM, with the PchB mutant K42A retaining just 1% of WT function.[5,15-19] Moreover, mutations made at K42 in PchB showed large effects on IPL activity with a 100-fold reduction in IPL activity for PchB mutant K42A and complete loss of function in the case of the charge swap mutation K42E.[5]

The PchB mutation results for K42A's IPL activity gives support to the second school of thought when it comes to how enzymes catalyze pericyclic reactions through the idea of what can referred to as reactive substrate destabilization by near attack conformation (NAC). The NAC is defined as a ground state conformation where the reactive groups of the substrate are within van der Waals contact radius at $\pm 15^{o}$ of the bonding angles of the transition state.[20] Binding of the substrate by the enzyme encourages this conformation change in the substrate, thereby allowing the substrate passage to the transition state without further input from the enzyme.[20-23] The PchB mutant K42A specifically addresses the idea of electrostatic interaction by removal of the positive charge in the from lysine at position 42. PchB has be shown to be a more versatile system for studying the contributions of electrostatic interactions and reactive

Figure 2-2. Active site view of chorismate mutases. *Panel A*, Active site of BsCM with TSA bound (PDB code: 2CHT). *Panel B*, Active site of EcCM with TSA bound (PDB code: 1ECM). *Panel C*, Active site of PchB mutant K42A with salicylate and pyruvate bound (PDB code:3HGX). Transition state analogue depicted in green sticks in panels A & B, salicylate and pyruvate depicted in cyan sticks in panel C.

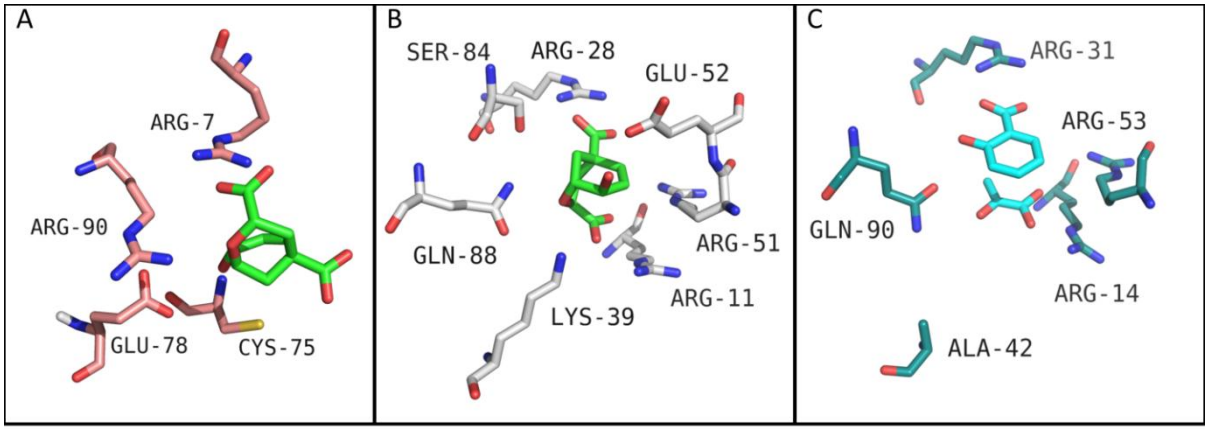

substrate stabilization towards pericyclic reactions then chorismate mutases as evident by the varying degrees of IPL activity achieved through mutational analysis carried out by Luo and co-workers as discussed in chapter 1.[5] Further exploration of the structural basis for the effects of mutations at lysine 42 in PchB is needed to specifically elucidate the contributions of various charged residues (K42, K42E, K42H) found to be important for efficient IPL activity.

In this chapter protein X-ray crystallography studies were carried out on WT PchB (K42) and mutant K42E to provide insight into the positioning of residue K42 with respect to the active site in WT PchB and the structural nature of the relative rate decrease for IPL activity in the PchB mutant K42E.[5] The results obtained provide structural evidence that that the relative rate decrease of PchB mutant K42E is not due to a change in the active site architecture of PchB, but more likely the result of the importance of positive charge in WT PchB at position 42 (lysine) relative to the negative charge found in the PchB mutant K42E. These results add to the insight of the role of transition state stabilization and reactive substrate destabilization in PchB.

2.2 Materials and Methods

Expression and Purification of Recombinant and WT PchB

The sub-cloning of the PchB expression plasmid has previously been reported.[5] Expression and purification of recombinant and WT PchB was performed as previously described[6] with the exception of substituting overnight growth at 15 ^{o}C instead of the previous three hours at 37 ^{o}C. Bacterial cells (*E. coli* BL21(DE3), Invitrogen) were grown in 1 liter non-baffled Fernbach flasks containing LB media at 37 °C with shaking at 250 rpm until an optical density of 0.8 at 600 nm was reached (Thermo-Fisher). The bacterial cells were induced with 0.2

mM isopropyl-β-D-thiogalactopyranoside (IPTG) and the incubator temperature was reduced to 15 ^{o}C for overnight growth. In the morning the bacterial cells were harvested by centrifugation at 4,000 x g for 10 min at 4 °C. Cells were resuspended with ~15 mL of buffer A (25 mM Tris-HCl (pH 8.0)) and lysed by sonication (Digital Sonifier, Branson) on ice for a total of 3 min consisting of 3 second bursts with intervening 20 sec resting periods. The lysed bacterial cells were subjected to ultracentrifugation at 142,000 x g for 45 min at 4 °C to remove cellular debris. The supernatant was applied to a 30Q Sepharose Fast Flow column (Amersham Biosciences) equilibrated with buffer A for anion-exchange chromatography. A linear gradient from 0 – 50% buffer B (25 mM Tris-HCl (pH 8.0), 500 mM NaCl) was applied to the 30Q column and PchB eluted at ~18% B. The fractions were analyzed using 15% SDS-PAGE and fractions containing PchB were pooled and concentrated to ~4 mL using a stirred cell apparatus (Amicon) with a YM-10 membrane (NMWL of 10 kDa) under nitrogen gas at 73 psi. The concentrated pooled fractions were applied to a HiLoad 16/60 Superdex 75 gel filtration column (GE Healthcare) equilibrated with 50 mM Tris-HCl pH 8.0, 150 mM NaCl, 10% glycerol and 1 mM DTT. The resulting fractions were analyzed using 15% SDS-PAGE and found to be of high purity (≥99%). The protein concentration was determined by Bradford assay using an IgG standard curve. Approximately ~250 mg of PchB was purified per liter of cell culture. The purified protein was aliquoted into Eppendorf tubes and stored at -80 ^{o}C for crystallization screens.

Rationale of Crystallization Screens of WT PchB and Recombinant Proteins

Crystallization trials were undertaken for WT and PchB mutants K42E, K42H and K42A. Based on previous studies of PchB[1,5,6] sparse matrix screening of apo, chorismate, prephenate, salicylate and pyruvate mixtures of WT and PchB mutants K42E, K42H and K42A were

established in hopes that crystals would form with the previously mentioned ligands bound in the active site. WT PchB incubated with chorismate would show CM activity yielding prephenate in the resultant crystal structure. WT PchB incubated with isochorismate would show IPL activity yielding pyruvate and salicylate in the resultant crystal structure. This would also apply to PchB mutants K42H and K42A albeit with lower turnover rates then WT PchB.[5] The PchB mutant K42E however showed no CM or IPL[5] activity potentially yielding four different crystal structures (apo, chorismate, prephenate, salicylate and pyruvate). Sparse matrix screening was carried out as shown in Table 2-1.

Screening and Optimization

Once a condition was found to produce crystal growth, optimization of that condition was undertaken to improve the size, geometry, number of nucleation sites and rate of crystal formation. This included trying various crystallization conditions to limit the rate of vapor diffusion between the mother liquor and protein drop which included physically changing the distance from the protein drop to the mother liquor by switching from a hanging drop to sitting drop geometry. This also included varying the size of the protein drop and also the ratio of the protein drop with respect to the mother liquor. Temperature was also considered an optimization variable and trays were setup 25, 18, and 14 ^{o}C. Streaking and seeding of PchB crystals into fresh protein drops to aid in nucleation was also performed. The most varied and useful optimization condition technique involved exploring various pH ranges around the initial hit in the sparse matrix screening. The optimization of the original sparse matrix screenings lead to enhanced rates of crystallization, size and geometry as shown in Figure 2-3.

Table 2-1. Table of sparse matrix crystallization screens for WT PchB and mutant K42E. The crystallization screens used in the crystallization of PchB are listed below. Both WT PchB and mutant K42E were incubated with reactants and products of PchB's IPL and CM activities. WT PchB and mutant K42E were also attempted to be crystallized in their apo form.

Protein	Protein Concetration (mg/mL)	Additive	Additive Concentration in Drop (mM)	Temperature 25 °C	Crystal Screen*	Crystal Screen 2*	Peg/Ion Screen*	Index*	Wizard I**	Wizard II**	Wizard III**	Wizard IV**
WT PchB	52.6	Salicylate & Pyruvate	20.6	X	X	X	X	X	X	X	X	
WT PchB	52.6	Chorismate	31.0	X	X	X	X	X	X	X	X	
WT PchB	52.6	Prephenate	16.7	X	X	X	X	X	X	X	X	
WT PchB	52.6	Apo	--	X	X	X	X	X	X	X	X	
PchB K42E	34.6	Salicylate & Pyruvate	14.2	X	X	X	X		X	X	X	X
PchB K42E	34.6	Chorismate	23.1	X	X	X	X		X	X	X	X
PchB K42E	34.6	Prephenate	12.0	X	X	X	X		X	X	X	X
PchB K42E	34.6	Apo	--	X	X	X	X		X	X	X	X

*Hampton Research Crystallization Screens **Emerald BioSystems Crystallization Screens

Figure 2-3. Time lapse images of WT PchB crystal growth. WT PchB crystals grew at an extraordinarily high rate in the presence of lithium sulfate (0.2 M), sodium acetate (0.1 M, pH 4.5), and glycerol (6%). Images were collected of WT PchB crystal growth in optimized mother liquor conditions. The frames below consist of a series of 20 images taken every 10 minutes over the course of 3 hours and 10 minutes. The birth of a new crystal is visible at time point 01:10:00 which progressively gets larger as time goes on. The scale of the bar in each frame is 125 um. WT PchB crystals would reach a maximal size ~24 hours post setup. Crystals of WT PchB were allowed to grow anywhere between 12 to 24 hours before harvesting.

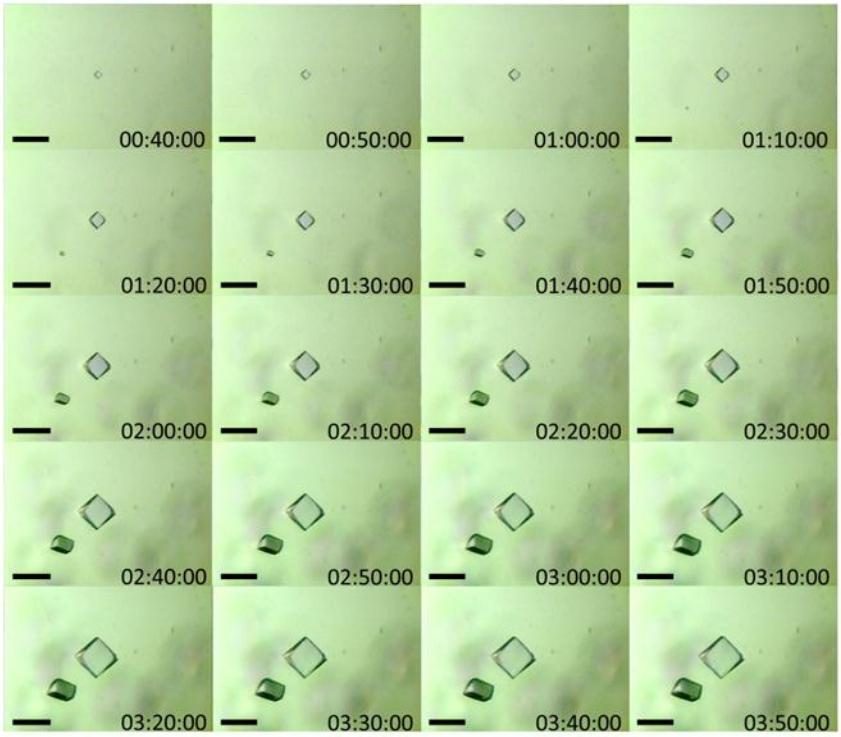

Optimization of Cryoprotectants for PchB Crystals

The original cryoprotectants screened consisted of mother liquor and increasing amounts of glycerol. All cryoprotectants were then flash cooled with liquid nitrogen to test their ability to form an amorphous glass and hence be a suitable choice of cryoprotectant for PchB. Upon transfer of PchB crystals from the hanging drop to suitable cryoprotectant drops fine lines appeared on the surface of the crystals after a short time period before flash cooling of crystals for data collection. This was believed to be the deterioration of the PchB lattice structure as the crystals yielded poor quality diffraction images consisting of heavy smearing and low angle diffraction (images not shown). Serial exposure of PchB crystals into progressively higher concentrations of glycerol tended to slow this effect, but did not completely eliminate the appearance of cracks with time. All visible cracks and fine lines were eliminated when the cryoprotectants contained roughly the same amount of salicylate and pyruvate as that found in the hanging drop crystallization conditions. WT PchB and mutant K42E crystals that were flashed cooled with cryoprotectants that contained salicylate and pyruvate yielded high resolution diffraction images (Figure 2-4) and subsequent molecular structures.

Crystallization Conditions for WT PchB and K42E Structures

WT PchB with Salicylate and Pyruvate.

Crystallization of WT PchB was carried out using the hanging drop vapor diffusion method at 25^{o} C. Purified WT PchB (64 mg/ml) was mixed with a salicylate-pyruvate solution in a 1:20 ratio of WT PchB to Salicylate and Pyruvate (Sal-Pyr, 2.9 mM: 58.0 mM) and incubated on ice for 30 min. Hanging drops consisted of 1.0 uL of the WT PchB-Sal-Pyr solution mixed with 1.0 uL of well solution containing 0.2 M lithium sulfate, 0.1 M sodium acetate (pH 4.5)

Figure 2-4. Diffraction and crystal images of WT PchB and mutant K42E. Below are the diffraction patterns obtained for WT PchB (top) and mutant K42E (bottom). Both show well dispersed singular spots to a high degree of resolution. The insets are representative crystals of WT PchB and mutant K42E used to produce the diffraction images. WT PchB crystal dimensions consisted of 0.12 x 0.12 x 0.05 mm while mutant K42E was slightly smaller at 0.06 x 0.06 x 0.04 mm. All diffraction data was collected using beam line 9-2 at the Stanford Synchrotron Radiation Lightsource.

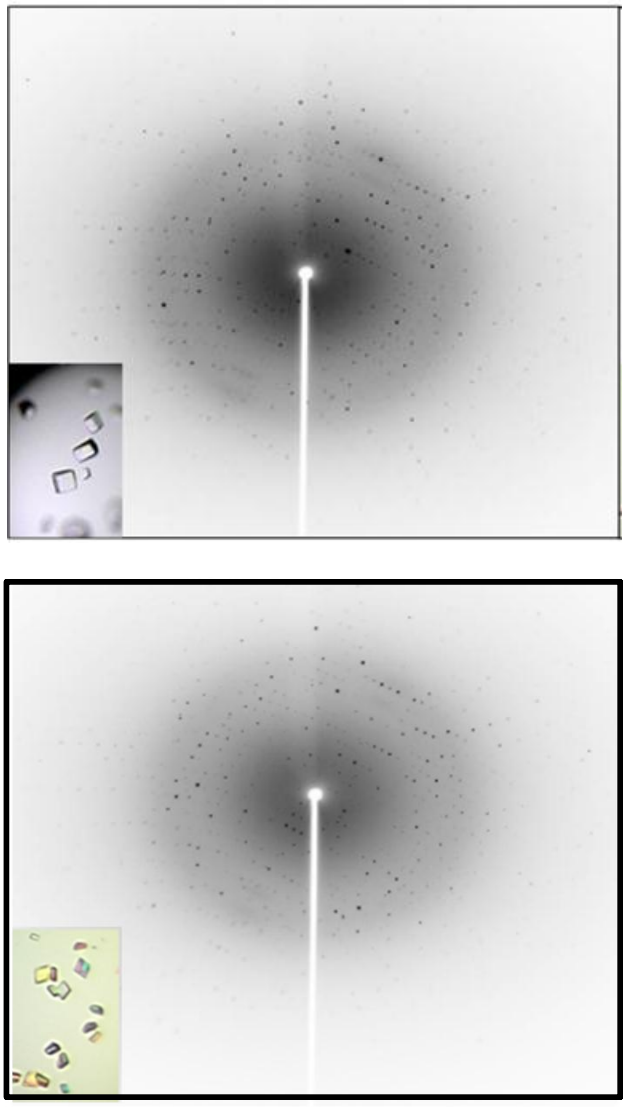

and 6% glycerol. Parallelepiped crystals grew to ~ 0.12 mm x 0.12 mm x 0.05 mm within twenty-four hours.

K42E PchB with Salicylate and Pyruvate.

Crystallization of the PchB mutant K42E was carried out using the hanging drop vapor diffusion method at 25^{o} C. Purified K42E (34 mg/ml) was mixed with a salicylate-puruvate solution in a 1:20 ratio of K42E to Sal-Pyr (2.9 mM: 58.0 mM) and incubated on ice for 30 min. Hanging drops consisted of 1.0 μL of the K42E-Sal-Pyr solution mixed with 1.0 μL of well solution containing 0.004 M Gly-Gly, 0.100 M sodium acetate (pH 3.6) and 12% glycerol. Parallelepiped crystals grew to ~ 0.06 mm x 0.06 mm x 0.04 mm in two days.

Collection of Crystallographic Data and Structure Determination for PchB

WT PchB with Salicylate and Pyruvate.

A WT PchB crystal was transferred to a drop containing 20% glycerol and flash cooled to -180^{o} C with liquid nitrogen. Diffraction data were collected remotely at beam line 9-2 at the Stanford Synchrotron Radiation Lightsource. The collected diffraction images consisted of 1^{o} oscillations with an exposure time of 20 sec and a detector distance of 290 mm (Figure 2-4). The diffraction data were indexed and scaled using the XDS program package.[24]

PchB K42E with Salicylate and Pyruvate.

A PchB K42E crystal was transferred to a drop containing 20% glycerol and flash cooled to -180^{o} C with liquid nitrogen. Diffraction data were collected remotely at beam line 9-2 at the Stanford Synchrotron Radiation Lightsource. The collected diffraction images consisted of 1^{o} oscillations with an exposure time of 15 sec and a detector distance of 100 mm (Figure 2-4). The diffraction data were indexed and scaled using the XDS program package.[24]

Structure Determination

Structure determination was performed by molecular replacement for both WT and K42E PchB using Phaser[25] from the CCP4[26] suite using the PchB pyruvate-bound structure (PDB Code: 2H9D) as a model with the water and ligands omitted. The resultant models were refined using Coot[27], Phenix[28] and REFMAC with resultant statistics (Table 2-2).

Table 2-2: Crystallographic Statistics

	WT†	K42E†
Data Collection		
Resolution Range (Å)[1]	31.71 - 1.95 (2.06 - 1.95)	25.89 - 1.79 (1.84 - 1.79)
Space Group	$P22_12_1$	$P2_12_12$
Unit Cell (Å)	a = 47.3, b = 60.3, c = 60.6	a = 46.1, b = 57.3, c = 60.3
Observations		
Unique	12,438	15,294
Total	45,612	54,206
Completeness (%)	95.6 (97.1)	97.2 (97.9)
Rsym[2]	0.058 (0.226)	0.098 (0.375)
$\langle I/\sigma(I) \rangle$	15.4 (5.2)	5.7 (2.0)
Refinement		
Resolution Range (Å)	31.71 - 1.95	25.89 - 1.79
Number of Reflections	11,177	13,690
R-factor [3]	0.230	0.207
R_{free}[4]	0.290	0.264
Dimers/asymmetric unit	1	1
Number of atoms		
Protein, nonhydrogen	1570	1529
Nonprotein	76	76
R.m.s. deviations		
Length (Å)	0.011	0.022
Angles (°)	1.21	1.87
Overall B factor ($Å^2$)	16.3	20.9
Protein	16.3	20.6
Sal & Pyr	14.8	27.0
Water	18.3	26.0

[1]Values in parentheses are for the highest resolution shell.

[2]$R_{sym} = \Sigma| I_{obs} - I_{avg} | / \Sigma I_{obs}$ where the summation is over all reflections.

[3]$R_{factor} = \Sigma| F_o - F_c | / \Sigma F_o$.

[4]For calculation of R_{free}, 10.0% (WT), and 10.1% (K42E) of the reflections were reserved.

†Salicylate and Pyruvate bound in the active site.

2.3 Results

Crystal Structure of WT PchB with Salicylate and Pyruvate Bound

The crystal structure of WT PchB with salicylate and pyruvate bound in the active site was determined to a resolution of 1.95 Å. The crystals of WT PchB belong to the space group $P22_12_1$. This WT PchB structure crystallized in a similar space group to previous apo WT PchB, PchB mutant K42A and I87T structures ($P2_12_12_1$).[5,6] The unit cell for WT PchB with salicylate and pyruvate bound was also different than those previously reported. The WT PchB structure consists of two chains (A and B) that form intertwined dimers that overall make a homodimer with two equivalent active sites (Figure 2-5, A). The two equivalent active sites were closed with one molecule of pyruvate and one molecule of salicylate bound in each. The WT PchB structure is overall well-ordered throughout with disordered regions only consisting of the N-terminal methionine and last three amino acids at the C-terminus (Table 2-3, G99, A100, A101). The salicylate and pyruvate in the active site are oriented by the carboxylate group of arginine 31 and arginine 14, respectively (Figure 2-5,C). The root mean squared deviation (RMSD) for the homodimer of WT PchB with salicylate- and pyruvate-bound compared to a homodimer of WT PchB with two pyruvate molecules bound in the active site is 0.27 Å for 196 α-carbons showing a highly conserved overall structure between the two wild-type forms. Comparing the α-carbon at residue 42 in both structures yields an RMSD of 0.53 Å[29]. This is higher than the overall structure but corresponds to previous RMSD values of residue 42 comparisons between the WT PchB (two pyruvate) and PchB mutant K42A structures.[5] The active site of WT PchB with salicylate and pyruvate is shown in stereo in Figure 2-5 allowing a clear view of the products of IPL activity and interacting amino acids.

Figure 2-5. Structure of WT PchB with salicylate and pyruvate bound and structural homologue EcCM with a transition state analog bound. *Panel A,* Global view of WT PchB with salicylate and pyruvate bound showing the active dimer with two equivalent active sites (PDB code: 3REM, The salicylate and pyruvate are shown as magenta sticks.) *Panel B,*Global view of PchB structural homologue EcCM with TSA bound (PDB code: 1ECM, The transition state analog is marine blue.) *Panel C,* Stereo image of the active site of WT PchB with $2|F_o|-|F_c|$ electron density (grey mesh) contoured at 1.0 σ around salicylate, pyruvate and water. Arginine 31 and arginine 14 align the carboxylates of salicylate (R31) and pyruvate (R14). Lysine 42 is hypothesized to play a role in transition state stabilization by supporting the developing negative charge on the substrate during catalysis. Amino acids are labeled with PchB numbering (Chain A: R31, K42, R53, Q90 Chain B: R14).

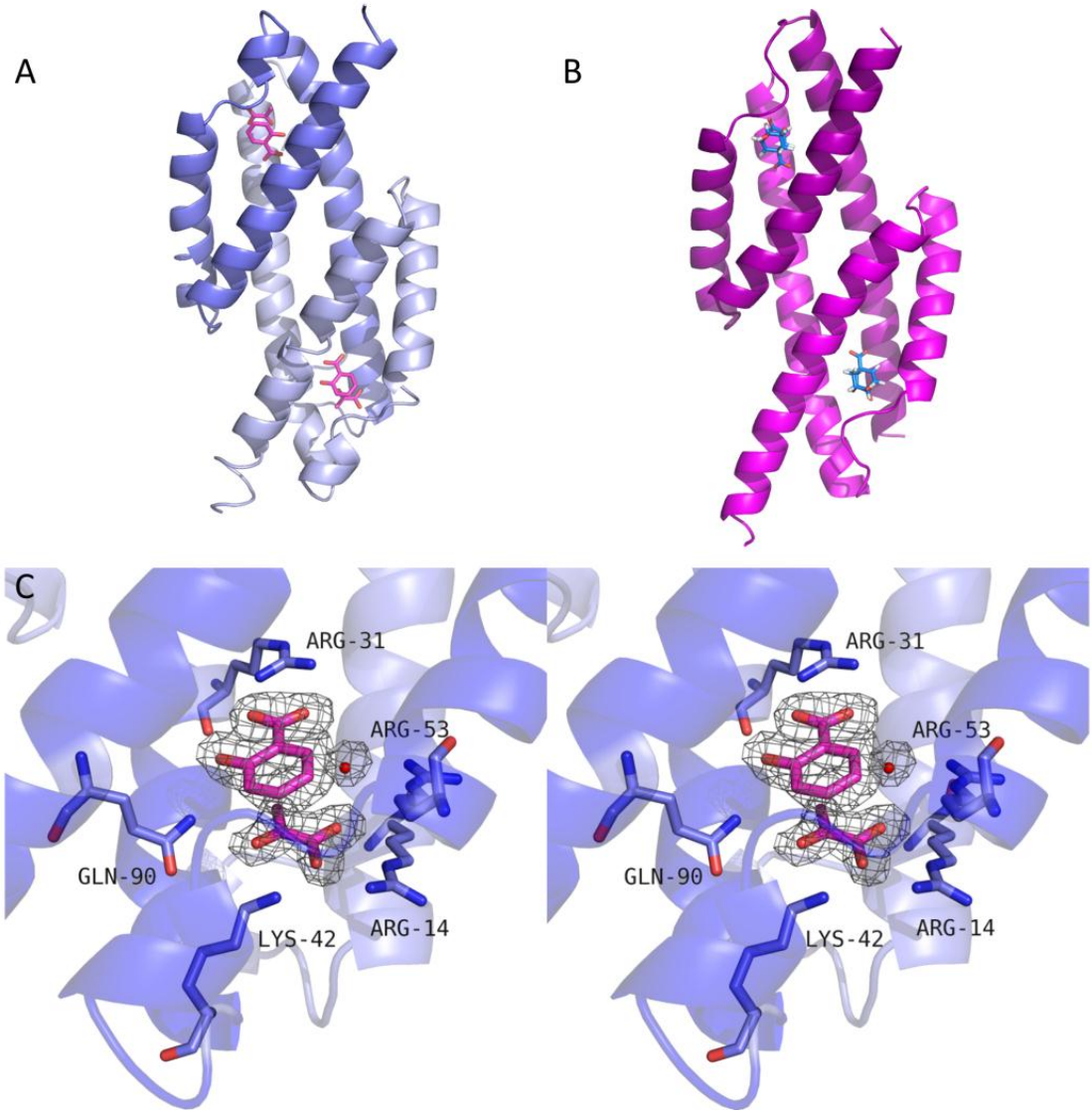

Table 2-3: Summary of WT and K42E Structures

	Ordered Regions	Ligands Bound in the Active Site
WT[†]		
Chain A	2-98	Salicylate and Pyruvate
Chain B	2-98	Salicylate and Pyruvate
K42E[†]		
Chain A	1-97	Salicylate and Pyruvate
Chain B	1-41, 48-97	Salicylate and Pyruvate

[†]Full length PchB consists of 101 amino acids

Crystal Structure of PchB mutant K42E with Salicylate and Pyruvate Bound

The crystal structure of PchB mutant K42E with salicylate and pyruvate bound in the active was determined to a resolution of 1.79 Å. The crystals of PchB mutant K42E belong to the space group $P2_12_12$. The space group of K42E is a similar space group to previous apo WT PchB, PchB mutant K42A and I87T ($P2_12_12_1$) structures.[5,6] The PchB mutant K42E is also slightly different than that of WT PchB with salicylate and pyruvate bound ($P22_12_1$) differing by one screw axis. The unit cell for K42E was different than those of previous PchB crystals but very similar to WT PchB with salicylate and pyruvate bound (WT a=47.3 b=60.3 c=60.6, K42E a=46.1 b=57.3 c=60.3). The K42E structure consists of chains A and B that form intertwined dimers that overall make a homodimer with two equivalent active sites (Figure 2-6,A). The active site is closed in both monomers with one molecule each of salicylate and pyruvate bound in each active site. The K42E structure is overall well-ordered throughout chain A with disordered regions consisting of only last 4 amino acids at the C-terminus (Table 2-3, R98, G99, A100, A101) and a portion of the chain B loop region consisting of E42 - I47. This disorder in the active site loop in chain B does not affect the binding of salicylate or pyruvate within the active site. The salicylate and pyruvate in the active site are oriented by the carboxylate group of arginine 31 and arginine 14 (Figure 2-6,C). The root mean squared deviation (RMSD) for the homodimer of WT PchB with salicylate- and pyruvate-bound compared to K42E was 0.29 Å for 188 α-carbons of the dimer showing a conserved overall structure between the two wild-type forms. Focusing on the α-carbon at residue 42 for chain A yields an RMSD of 0.34 Å.[29] The active site of PchB mutant K42E with salicylate and pyruvate is shown in stereo in Figure 2-6 allowing a clear view of the products of IPL activity and interacting amino acids.

Figure 2-6. Structure of PchB mutant K42E with salicylate and pyruvate bound with comparative WT PchB. *Panel A,* Global view of PchB mutant K42E with salicylate and pyruvate bound (cyan sticks) showing the active dimer with two equivalent active sites (PDB code: 3RET). *Panel B,* Global view of WT PchB with salicylate and pyruvate bound (magenta sticks) showing the active dimer with two equivalent active sites (PDB code: 3REM). *Panel C,* Stereo image of the active site of PchB mutant K42E with $2|F_o|-|F_c|$ electron density (grey mesh) contoured at 1.0 σ around salicylate, pyruvate and water. Arginine 31 and arginine 14 align the carboxylates of salicylate (R31) and pyruvate (R14). The K42E mutation is hypothesized to disrupt transition state stabilization by repelling the developing negative charge on the substrate during catalysis. Amino acids are labeled with PchB numbering (Chain A: R31, K42, R53, Q90 Chain B: R14).

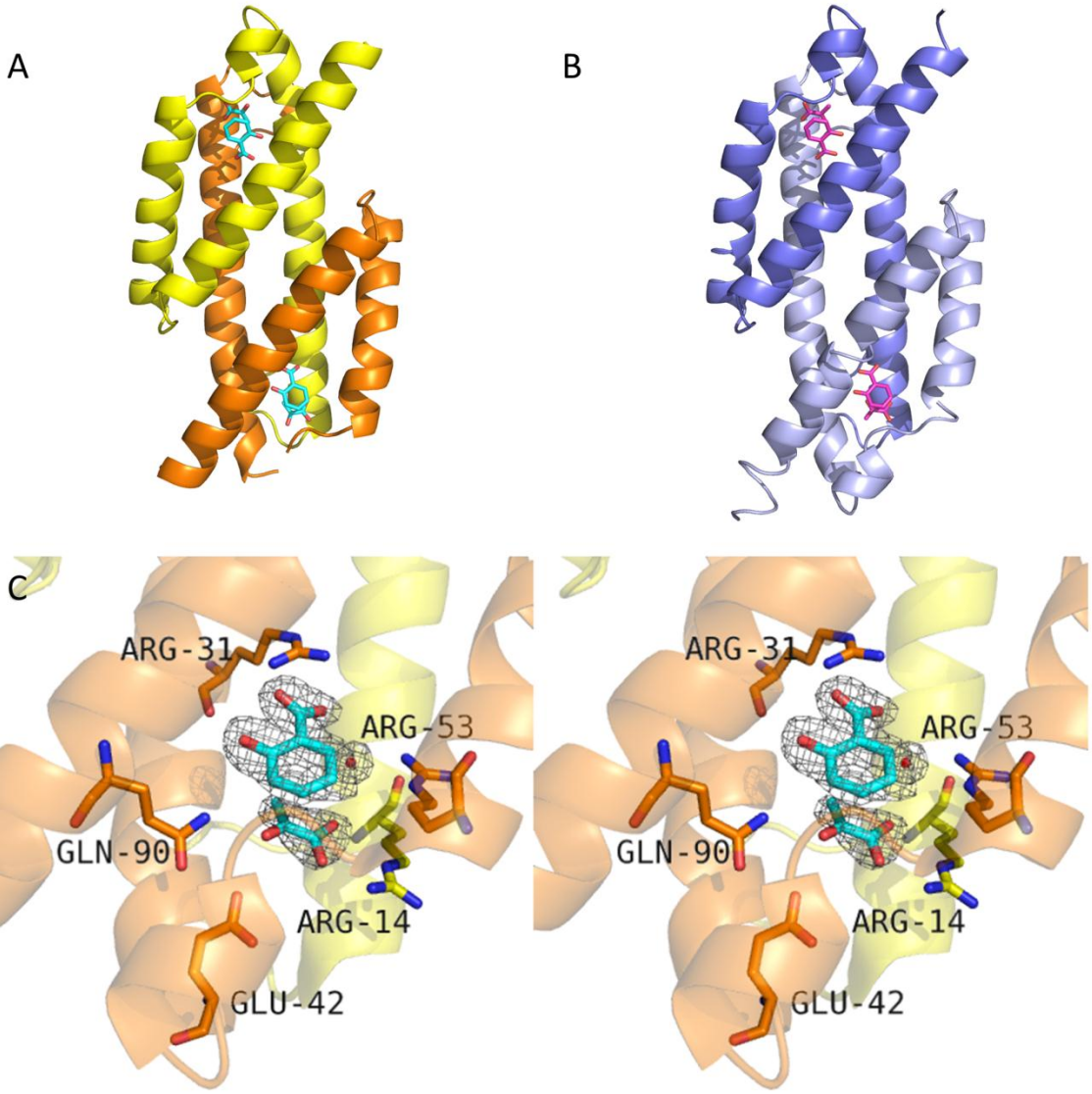

2.4 Discussion

Comparison of WT PchB Structures (2Pyr and Sal & Pyr)

The stereo overlay of the two WT PchB structures (PDB codes: 3REM, 2H9D) show a good agreement of the overall active site architecture (Figure 2-7). One noticeable difference is in the position of R53 in the WT PchB with 2 molecules of pyruvate bound (2H9D) structure (green sticks) relative to that of R53 in the WT PchB with salicylate and pyruvate bound structure (3REM). The side chain is flipped in towards the pyruvate molecules bound in the active site (yellow sticks). In the WT PchB with salicylate and pyruvate structure the flipped R53 is replaced by a water molecule that appears to provide the same hydrogen bonding network in place of R53. The carboxylic group of the two pyruvates are organized in the active site by R31 and R14 in the WT PchB structure with two molecules of pyruvate bound which is consistent with the organization of salicylate (R31) and pyruvate (R14) in the WT PchB salicylate and pyruvate bound structure. Another slight difference between the two structures is in the position of glutamine 90. In the 2H9D structure the glutamine is position to interact specifically with only one pyruvate molecule, which is in contrast to the 3RET structure where glutamine 90 is position to interact with not only pyruvate but also salicylate. The relative position of K42 is shared among the two crystal structures. The position of K42 within both structures places it in proximity of stabilizing the developing negative charge on the ether oxygen during the transition state of PchB's IPL activity. Overall the active site architecture is conserved among both structures. Even with the presence of salicylate, with its aromatic ring structure, there are no drastic changes in the active site architecture. This new view of WT PchB with salicylate and pyruvate bound in the active site shows the conserved interactions while at the same time shows

Figure 2-7. Stereo overlay comparing the active sites of two WT PchB crystal structures. WT PchB with salicylate and pyruvate bound (blue and magenta sticks, PDB Code: 3REM). WT PchB with two molecules of pyruvate bound (green and yellow sticks, PDB Code: 2H9D). Arginine 31 and arginine 14 align the carboxylates of salicylate (R31) and pyruvate (R14) in 3REM and also both pyruvate molecules in 2H9D. Lysine at position 42 is hypothesized to aid in transition state stabilization by supporting the developing negative charge on the substrate during catalysis. Differences in the active site architecture include positioning of arginine 53 in 2H9D (green sticks) relative to the water arginine 53 position in 3REM (red sphere, blue sticks). Amino acids are labeled with PchB numbering (Chain A: R31, K42, R53, Q90, Chain B: R14).

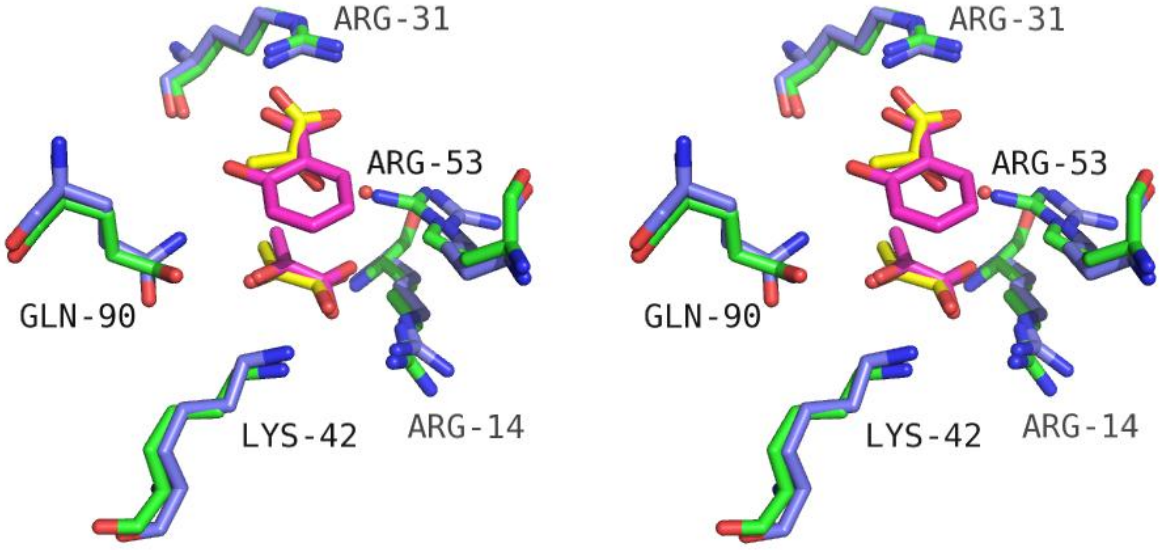

the conserved interactions while at the same time showing the subtle differences between these two structures.

Comparison of WT PchB (Sal & Pyr) & K42E Structures

Comparison of the active sites for the crystal structures for WT PchB (blue sticks) and PchB mutant K42E (orange sticks) also shows a highly conserved active site architecture (Figure 2-8). This comes as a surprise because due to the recent mutational analysis study by Luo and co-workers that reports no detectable IPL or CM activity for the PchB mutant K42E.[5] Both arginines at position 31 orient the carboxylic group of salicylate within the active site. The pyruvate is also oriented in the active site by carboxylic interactions with arginine 14. The major difference between these two structures is in the length of the variant side chain of glutamic acid at position 42 relative to that of the native lysine in the WT structure and the charge carried by both residues.

Comparison of K42E (Sal & Pyr) with K42A (Sal & Pyr)

Comparison of the PchB mutant structures K42E (PDB code: 3RET, orange sticks) and K42A (Pdb code: 3HGX, pink sticks) also shows a conserved active site architecture (Figure 2-9) between both structures. The salicylate and pyruvate molecules are orientated in the active site by the same interactions of their carboxylic acid groups with arginines 31 and 14 in both structures. The most noticeable difference is in the length of the side chain at position 42.

Figure 2-8. Stereo overlay comparing the active sites of WT PchB and K42E crystal structures. WT PchB with salicylate and pyruvate bound (blue and magenta sticks, PDB Code: 3REM). PchB mutant K42E with salicylate and pyruvate bound (orange and cyan sticks, PDB Code: 3RET). Arginine 31 and arginine 14 align the carboxylates of salicylate (R31) and pyruvate (R14) in 3REM and 3RET. The lysine at position 42 in 3REM is hypothesized to aid in transition state stabilization while the glutamic acid in 3RET represents a charge swap debilitating for transition state stabilization. The overall active site architecture and positioning of salicylate and pyruvate remain consistent in both structures. Amino acids are labeled with PchB numbering (Chain A: R31, K42/E42, R53, Q90, Chain B: R14).

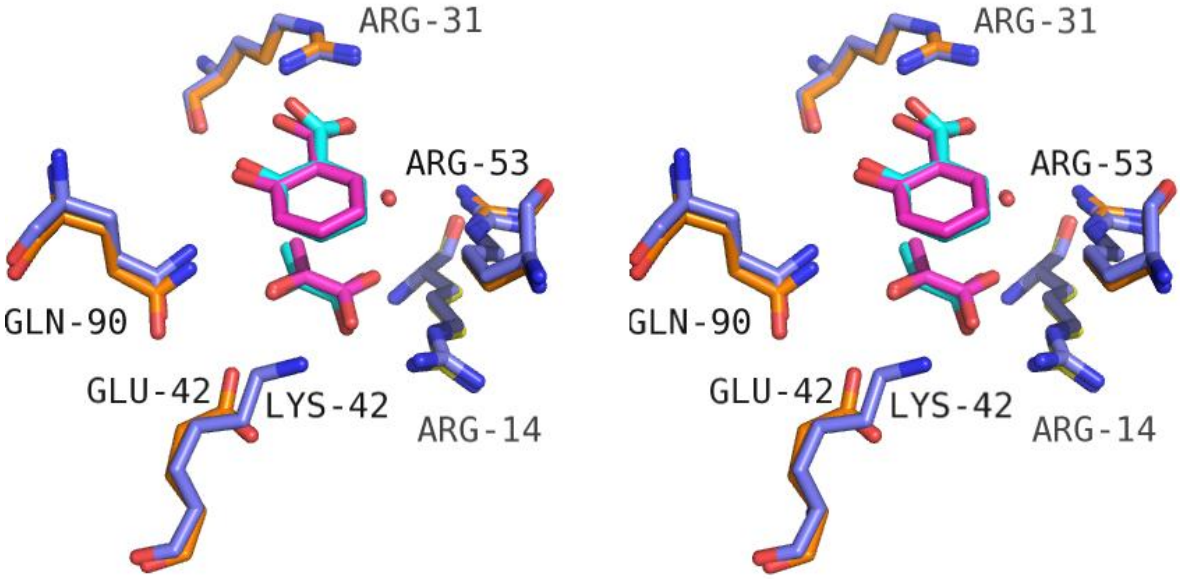

Figure 2-9. Stereo overlay comparing the active sites of PchB mutants K42E and K42A crystal structures. PchB mutant K42E with salicylate and pyruvate bound (orange and cyan sticks, PDB Code: 3RET). PchB mutant K42A with salicylate and pyruvate bound (magenta and green sticks, PDB Code: 3HGX). Arginine 31 and arginine 14 are shown to align the carboxylates of salicylate (R31) and pyruvate (R14) in 3RET and 3HGX. The glutamic acid at position 42 in 3RET represents a charge swap with debilitating effects to transition state stabilization. The alanine at position 42 represents an absence of supporting charge compared to WT PchB and mutant K42E. The overall active site architecture and positioning of salicylate and pyruvate remain consistent in both K42E and K42A mutant structures. Amino acids are labeled with PchB numbering (Chain A: R31, E42/A42, R53, Q90, Chain B: R14).

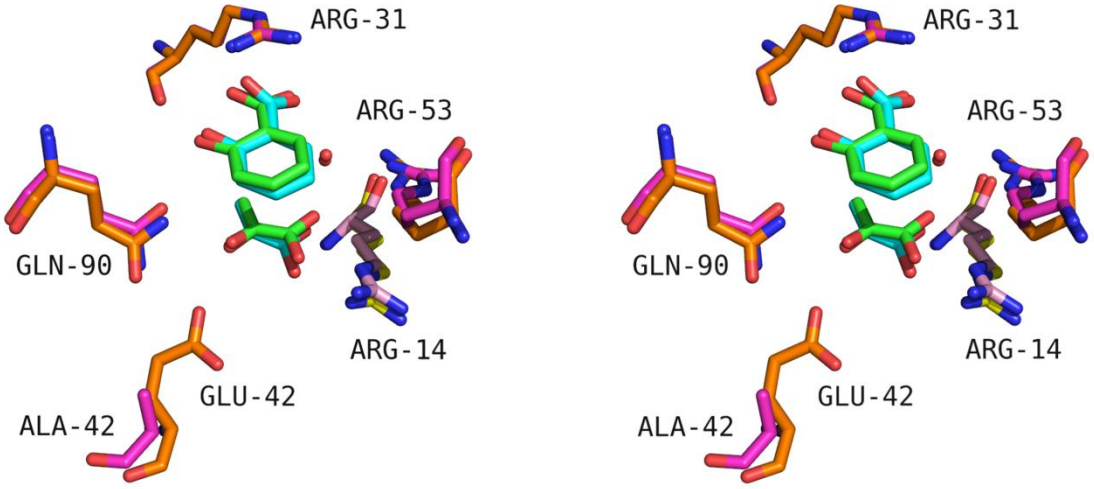

Comparison of WT PchB and Mutant Active Site Surface Area

Analysis of the electrostatic surface area has provided a detailed look at importance of charged residues at position 42 in PchB. CASTp[30] calculations performed on the active site surface area of WT PchB and mutants K42E and K42A yield an electrostatic surface area image of what can be imagined as a wine bottle with cork appearance (Figure 2-10). When the active site loop is ordered as is the case of residues at position 42 (Figure 2-10, A-C). The side chains directly position themselves into the active site of PchB. One major difference is the "un-corked" appearance of the active site in the case of PchB mutant K42A (Figure 2-10, C). The lysine to alanine mutation has physically shortened the side chain at position 42, resulting in an ordered active site loop region upon ligand binding, but at the same time exposing the active site to the surrounding solvent. This is in contrast to the K42E mutation which closes off the active site from the surrounding solvent when the active site loop is ordered (Figure 2-10, B). The K42E mutant however provides a strong negative charge as opposed to the positive charge found with lysine at position 42 in WT PchB (Figure 2-10, A). It is important to note that the K42A mutation decreases the IPL and CM activity 100-fold while the K42E mutant has no detectable activity for either IPL or CM activity.[5]

Figure 2-10. Interior view of the PchB active site. The calculated CASTp interior electrostatic surface area of PchB is shown for WT PchB and two mutants. *Panel A,* WT PchB with salicylate bound (PDB code: 3REM). *Panel B,* PchB mutant K42E with salicylate and pyruvate bound (PDB code: 3RET). *Panel C,* PchB mutant K42A with salicylate and pyruvate bound (PDB code: 3HGX). Notice the visible hole for K42A showing access to the surrounding solvent. Neutrally charged surface area represented by green (Panel A), cyan (Panel B) and magenta (Panel C). Notice the position of K42 directed towards the pyruvate in panel A and K42E in panel B.

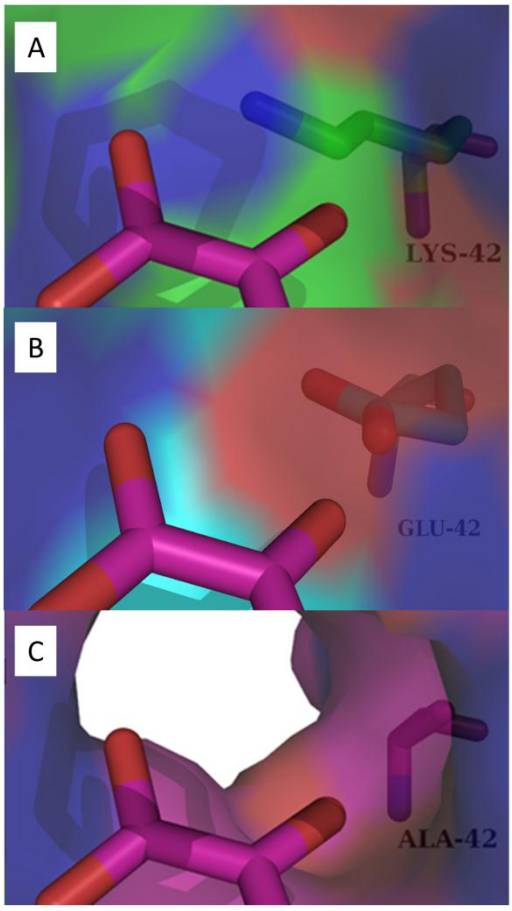

The Conserved Active Site Architecture of PchB

The WT PchB and the PchB mutants show a conserved active site architecture that does not drastically change among the individual mutants. This is the result of the arginines 31 and 53 correlating the carboxylates of the salicylate and pyruvate in the active site. These two interactions are fundamental in the stabilization of the products in the active site and therefore can be viewed as important for the binding of the substrate in the active site. These two interactions do not change among the mutants and so the major contributors orienting the substrate in the active site do not change. Even when the side chain length is drastically reduced, as in the case of the PchB mutant K42A, the active site loop is ordered and pyruvate and salicylate are oriented in the same manner with very little difference in the α-carbon at position 42 (Figure 2-11). The various lengths of the side chains themselves also show no overall apparent change in the active site architecture (Figure 2-11). The various lengths of WT, K42E and K42A PchB side chains represent major differences in the IPL and CM activity of PchB but are not by themselves structurally significant when stabilizing the products of IPL activity in the active site (Figure 2-11).

If the active site architecture is the same among WT PchB and mutant structures when stabilizing the products of IPL activity then the differences in activity are likely the result of the charge at position 42 and the dynamics of the active site loop. The initial binding event between the substrate and enzyme can be hypothesized to be mainly coordinated by the two arginines (R31 and R53) within the active site. We know that the active site loop has been shown to be ordered in the presence of substrate.[6] This ordering of the active site loop consequently aligns the charged residue at position 42 into the active site as shown with the previous crystal structures above along with an interaction necessary for PchB activity[5,6]. Once the substrate isochorismate

Figure 2-11. Overlay comparing the active sites of WT PchB and PchB mutants K42E and K42A. WT PchB with salicylate and pyruvate bound (blue and magenta sitcks, PDB code: 3REM). PchB mutant K42E with salicylate and pyruvate bound (orange and cyan sticks, PDB Code: 3RET). PchB mutant K42A with salicylate and pyruvate bound (magenta and green sticks, PDB Code: 3HGX). Arginine 31 and arginine 14 are shown to align the carboxylates of salicylate (R31) and pyruvate (R14). The overall active site architecture and positioning of salicylate and pyruvate remain consistent in both WT PchB and PchB K42E and K42A mutant structures. Notice the difference in physical length among the side chains at position 42. Amino acids are labeled with PchB numbering (Chain A: R31, K42/E42/A42, R53, Q90, Chain B: R14).

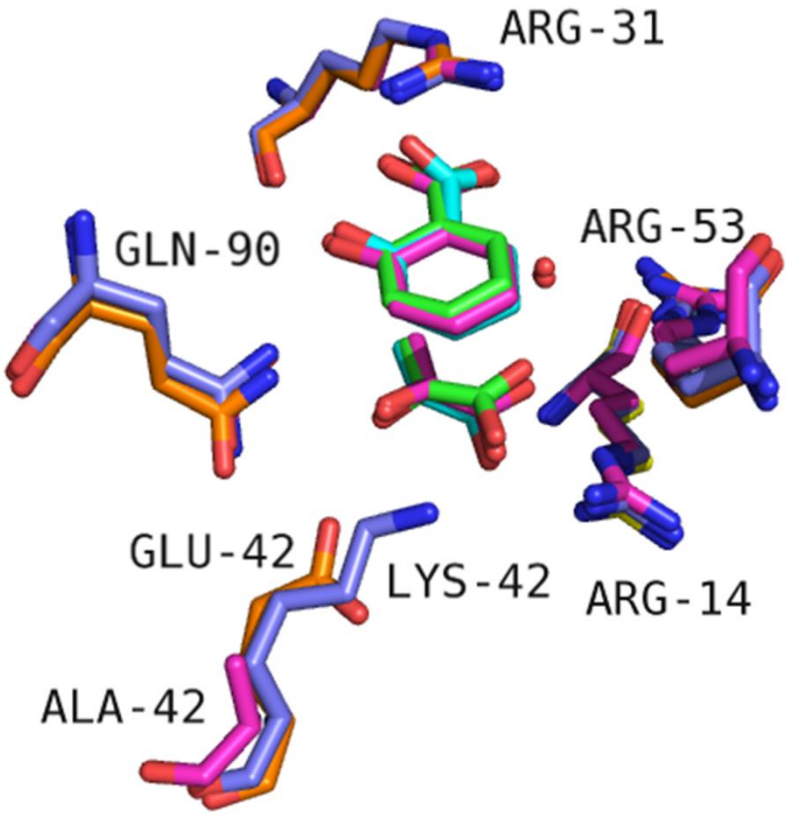

has passed through the transition state, the stabilization of the products within the active site are similar among WT PchB and PchB mutants. This highlights the importance of providing the correct charge at position 42 prior to catalysis allowing for IPL and CM activity to proceed. Whereas the placement of the positive charge in K42 is hypothesized to stabilize the developing negative charge on the ether oxygen of isochorismate, the placement of a negative charge in K42E can be hypothesized to destabilize the transition state through electrostatic interactions.[5,18] While the positive charge at position 42 has been shown to be the most efficient, the PchB mutant K42A still provides sufficient stabilization of the transition state allowing for IPL and CM activity, albeit at a reduced rate.[5]

The evidence for the importance of the correct charge at position 42 allowing for efficient catalysis is complimented by the ordered loop region upon ligand binding[6] with alignment of the charged residue at position 42 and subsequent release of the products once catalysis occurs. The structural studies so far have provided evidence for the importance of residue 42 while also raising the question of how loop dynamics are responsible for the positioning of residue 42 and therefor contribute to catalysis.

References

1. Gaille, C., Kast, P. & Haas, D. Salicylate biosynthesis in *Pseudomonas aeruginosa*. Purification and characterization of PchB, a novel bifunctional enzyme displaying isochorismate pyruvate-lyase and chorismate mutase activities. *J Biol Chem* **277**, 21768-21775 (2002).
2. Gaille, C., Reimmann, C. & Haas, D. Isochorismate synthase (PchA), the first and rate-limiting enzyme in salicylate biosynthesis of *Pseudomonas aeruginosa*. *J Biol Chem* **278**, 16893-16898 (2003).
3. DeClue, M.S., Baldridge, K.K., Kunzler, D.E., Kast, P. & Hilvert, D. Isochorismate pyruvate lyase: a pericyclic reaction mechanism? *J Am Chem Soc* **127**, 15002-15003 (2005).
4. Rajagopalan, J.S., Taylor, K.M. & Jaffe, E.K. 13C NMR studies of the enzyme-product complex of *Bacillus subtilis* chorismate mutase. *Biochemistry* **32**, 3965-3972 (1993).
5. Luo, Q., Olucha, J. & Lamb, A.L. Structure-Function Analyses of Isochorismate-Pyruvate Lyase from *Pseudomonas aeruginosa* Suggest Differeing Catalytic Mechanisms for the Two Pericyclic Reactions of This Bifunctional Enzyme. *Biochemistry* **48**, 5239-5245 (2009).
6. Zaitseva, J., Lu, J., Olechoski, K.L. & Lamb, A.L. Two crystal structures of the isochorismate pyruvate lyase from *Pseudomonas aeruginosa*. *J Biol Chem* **281**, 33441-33449 (2006).
7. Andrews, P.R., Smith, G.D. & Young, I.G. Transition-state stabilization and enzymic catalysis. Kinetic and molecular orbital studies of the rearrangement of chorismate to prephenate. *Biochemistry* **12**, 3492-3498 (1973).
8. Hilvert, D., Carpenter, S.H., Nared, K.D. & Auditor, M.T. Catalysis of concerted reactions by antibodies: the Claisen rearrangement. *Proc Natl Acad Sci U S A* **85**, 4953-4955 (1988).
9. Copley, S.D. & Knowles, J.R. The Uncatalyzed Claisen Rearrangement of Chorismate to Prephenate Prefers a Transition-State of Chairlike Geometry. *J Am Chem Soc* **107**, 5306-5308 (1985).
10. Copley, S.D. & Knowles, J.R. The Conformational Equilibrium of Chorismate in Solution - Implications for the Mechanism of the Nonenzymatic and the Enzyme-Catalyzed Rearrangement of Chorismate to Prephenate. *J Am Chem Soc* **109**, 5008-5013 (1987).
11. Warshel, A. Energetics of Enzyme Catalysis. *Proc Natl Acad Sci U S A* **75**, 5250-5254 (1978).
12. Warshel, A. *et al.* Electrostatic basis for enzyme catalysis. *Chemical Reviews* **106**, 3210-3235 (2006).
13. Lee, A.Y., Karplus, P.A., Ganem, B. & Clardy, J. Atomic structrue of the buried catalytic pocket of *Escherichia coli* chorismate mutase. *J Am Chem Soc* **117**, 3627-3628 (1995).
14. Lee, A.Y., Stewart, J.D., Clardy, J. & Ganem, B. New insight into the catalytic mechanism of chorismate mutases from structural studies. *Chem Biol* **2**, 195-203 (1995).
15. Liu, D.R., Cload, S.T., Pastor, R.M. & Schultz, P.G. Analysis of active site residues in *Escherichia coli* chorismate mutase by site-directed mutagenesis. *J Am Chem Soc* **118**, 1789-1790 (1996).
16. Cload, S.T., Liu, D.R., Pastor, R.M. & Schultz, P.G. Mutagenesis study of

active site residues in chorismae mutase from *Bacillus subtilis*. *J Am Chem Soc* **118**, 1787-1788 (1996).
17. Kast, P., Asif-Ullah, M., Jiang, N. & Hilvert, D. Exploring the active site of chorismate mutase by combinatorial mutagenesis and selection: the importance of electrostatic catalysis. *Proc Natl Acad Sci U S A* **93**, 5043-5048 (1996).
18. Kast, P. et al. A strategically positioned cation is crucial for efficient catalysis by chorismate mutase. *J Biol Chem* **275**, 36832-36838 (2000).
19. Kienhofer, A., Kast, P. & Hilvert, D. Selective stabilization of the chorismate mutase transition state by a positively charged hydrogen bond donor. *J Am Chem Soc* **125**, 3206-3207 (2003).
20. Hur, S. & Bruice, T.C. Comparison of formation of reactive conformers (NACs) for the Claisen rearrangement of chorismate to prephenate in water and in the *E. coli* mutase: the efficiency of the enzyme catalysis. *J Am Chem Soc* **125**, 5964-5972 (2003).
21. Zhang, X. & Bruice, T.C. A definitive mechanism for chorismate mutase. *Biochemistry* **44**, 10443-10448 (2005).
22. Hur, S. & Bruice, T.C. Just a near attack conformer for catalysis (chorismate to prephenate rearrangements in water, antibody, enzymes, and their mutants). *J Am Chem Soc* **125**, 10540-10542 (2003).
23. Hur, S. & Bruice, T.C. The near attack conformation approach to the study of the chorismate to prephenate reaction. *Proc Natl Acad Sci U S A* **100**, 12015- 12020 (2003).
24. Kabsch, W. XDS. *Acta Cryst.* D **66**, 125-132 (2010).
25. McCoy A.J., *et al.* Phaser crystallographic software. *J Appl Cryst* **40**, 658-674 (2007).
26. "The CCP4 Suite: Programs for Protein Crystallography". *Acta Cryst* D **50**, 760-763 (1994).
27. Emsley, P. and Cowtan, K. *Acta Cryst* D **60**, 2126-2132 (2004).
28. Adams, P., *et al.* PHENIX: a comprehensive Python-based system for macromolecular structure solution. *Acta Cryst* D **66**, 213-221 (2010).
29. Kleywegt, G.J., & Jones, T.A. Detecting folding motifs and similarities in protein structures. *Methods in Enzymology* **277**, 525-545 (1997).
30. Dundas, J. *et al.* CASTp: computed atas of surface topography of proteins with structural and topographical mapping of functionally annotated residues. *Nucl Acids Res* **34**, 116-118 (2006).

CHAPTER 3

Nuclear Magnetic Resonance Relaxation Studies of the PchB Mutant K42H

3.1 Introduction

Conformational changes and the macromolecular motions of an enzyme upon binding of a substrate contribute to moving the substrate farther down the reaction coordinate path towards the transition state.[1,2] These macromolecular motions vary in length from tenths to tens of angstroms and can vary in time from sub-pico seconds to over a second in length.[1] How much then do conformational changes and macromolecular motion contribute to the formation of the transition state when the transition state itself is estimated to exist for a mere 100 femtoseconds?[2] In chapter 1 we discussed how rate enhancement is proportional to how well an enzyme binds the transition state for a given substrate.[3] Applying this directly to the mutational studies performed on PchB at residue K42 would lead one to believe that decreases in catalytic rate[4] are fundamentally related to how well PchB can bind the transition state for isochorismate pyruvate lyase (IPL) and chorismate mutase (CM) activity. Positioning of residue K42 within the active site loop then brings into question how the dynamics of the active site loop region effect the rate of catalysis.

Dynamics of the Active Site Loop in PchB

The active site loop region of PchB (residues 39-51, monomers A &B) has been shown to be quite flexible.[5] The apo crystal structure of PchB (PDB code: 2H9C) shows a disordered active site loop region for both monomers, with one of the two equivalent active sites shown in Figure 3-1A. Well defined electron density around the active site exists for amino acids on both sides of the active site loop. The region associated with the active site loop in Figure 3-1A shows no electron density with magenta amino acids marking the beginning and end of the missing electron density. The lack of electron density for the loop region in the apo structure is the result of averaging the individual positions of each active site loop for all PchB molecules within the given crystal used for structure determination through x-ray diffraction. This is to say that the active site loop region adopts many distinct positions over time within any population of apo PchB molecules, resulting in weak diffraction and thereby producing electron density that is a blurred view of all super positions with no definable regions[6]. This is in direct contrast to the electron density found in the WT PchB crystal structure with pyruvate bound in the active site as shown in Figure 3-1, B (PDB code: 2H9D).[5] In this case, the ordered active site loop region shows well defined electron throughout the active site loop region. Also noticeable is the appearance of two pyruvate molecules with in the active site. This ordering of the active site loop was hypothesized to occur when a ligand is bound within the active site of PchB.[5] This hypothesis has been shown to be the case for previous K42A[3] (salicylate and pyruvate bound) and current WT PchB (salicylate and pyruvate bound) and K42E (salicylate and pyruvate bound) crystal structures.

Figure 3-1. View of the active site loop region in crystal structures of apo WT PchB and WT PchB with pyruvate bound. The pyruvate is green sticks. *Panel A,* Active site loop region of apo WT PchB (orange sticks: monomer B, cyan sticks: monomer A) showing one of two equivalent active sites with $2|F_o|-|F_c|$ electron density (grey mesh) contoured at 1.0 σ around the residues (PDB code: 2H9C). Missing active site loop region is highlighted with magenta residues. *Panel B,* Ordered active site loop region of WT PchB (yellow sticks: monomer A, blue sticks: monomer B) with pyruvate bound showing one of two equivalent active sites with $2|F_o|-|F_c|$ electron density (grey mesh) contoured at 1.0 σ around the residues and two pyruvate molecules (PDB code: 2H9D). Active site residue K42 is shown in green with two pyruvate molecules and magenta residues are used as reference for Panel A.

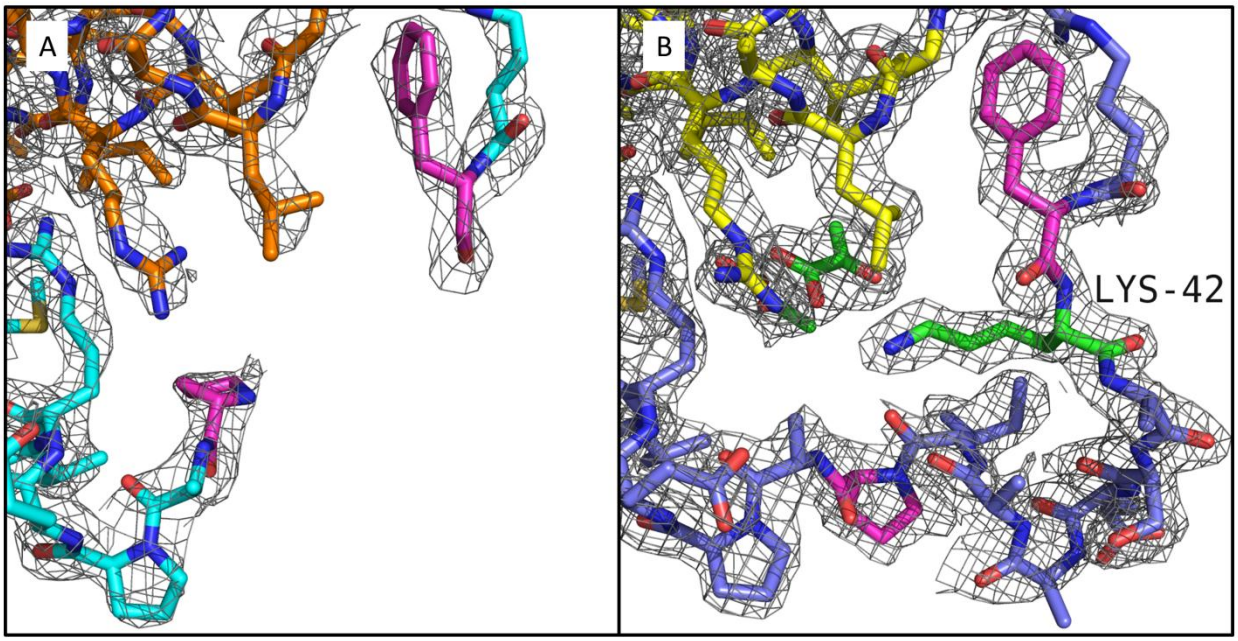

Coordination of Salicylate and Pyruvate in the Active Site

The coordination of salicylate and pyruvate (IPL products) in the active site of PchB has been shown to be facilitated by two arginines (R14 & R31) in the active site pocket of the crystal structure of PchB mutant K42A.[4] The K42A structure has completely negated the positive charge at position 42 in WT PchB and consequentially exhibits a 100-fold decrease in activity for both IPL and CM activity.[4] The significance of activity without electrostatic interactions from residue 42 within the flexible active site loop support the hypothesis that the active site loop contributes to catalysis through stabilizing the transition state. How much does the active site loop move in the presence and absence of substrate is yet to be determined.

In this chapter Nuclear Magnetic Resonance (NMR) experiments were carried out to provide insight into the relationship between dynamic active site loop movement and catalysis in PchB. The backbone resonance assignments were obtained from collections of 2D ^{1}H-^{15}N heteronuclear single-quantum coherence (HSQC)[8] and HNCA[9], CBCA(CO)NH[9], HNCACB[10] 3D data sets in combination with ^{15}N alanine and ^{15}N leucine labeled HSQC[11] experiments. These results lay the ground for determining the relative contributions of WT and PchB mutants in position 42 of the active site loop region towards stabilizing the transition or generation of a NAC.

3.2 Materials and Methods

Expression and Purification of ^{13}C-,^{15}N- and ^{15}N-labeled recombinant and WT PchB

The sub-cloning of the PchB expression plasmid has previously been reported.[4] Expression and purification of double labeled (^{13}C-, ^{15}N-) and single labeled (^{15}N-) recombinant

and WT PchB was performed as previously described[5] with modifications. Uniformly ^{13}C, ^{15}N- and ^{15}N-labeled PchB were obtained from bacterial cells *(E. coli* BL21(DE3), BL21 Star (DE3)pLysS, Invitrogen) that were grown up in 1 liter non-baffled Fernbach flasks containing minimal media supplemented with 2g/L of [^{13}C]-glucose for double labeled or 4g/L of glucose for single labeled sample with 1g/L [^{15}N]-ammonium chloride at 37 °C with shaking at 250 rpm until an optical density of 0.8 at 600 nm was reached (Cary 50 UV-Visible Spectrophotometer). The bacterial cells were induced with 0.2 mM isopropyl-β-D-thiogalactopyranoside (IPTG) and transferred to a 15 ^{o}C incubator with shaking at 250 rpm for overnight growth. Cells were harvested by centrifugation at 4,000 x g for 10 min at 4 °C. The pelleted bacterial cells were resuspended with ~15 mL buffer A (25 mM Tris-HCl (pH 8.0)) and lysed by sonication (Digital Sonifier, Branson) on ice for a total of 3 min consisting of 3 second bursts with intervening 20 sec resting periods. The lysed bacterial cells were subjected to ultracentrifugation at 142,000 x g for 45 min at 4 °C to remove cellular debris. The supernatant (~30 mL) was diluted to 150 mL with buffer A before being applied to a 30Q Sepharose Fast Flow column (Amersham Biosciences) equilibrated with buffer A for anion-exchange chromatography. A linear gradient from 0 – 50% buffer B (25 mM Tris-HCl (pH 8.0), 500 mM NaCl) was applied to the 30Q column and PchB eluted at ~18% B into 6 mL fractions. The fractions were analyzed using 15% SDS-PAGE and those containing PchB were pooled and concentrated to ~4 mL using a stirred cell apparatus (Amicon) with a YM-3 membrane (NMWL of 3 kDa) under nitrogen gas at 73 psi. The concentrated pooled fractions were applied to a HiLoad 16/60 Superdex 75 gel filtration column (GE Healthcare) equilibrated with 50 mM Tris-HCl (pH 8.0), 150 mM NaCl, and 10% glycerol. The resulting fractions were analyzed using 15% SDS-PAGE and found to be of high purity (≥99%). The protein concentration was determined by UV absorbance at 280 nm after

treatment with 6M guanidine-HCl. The purified protein was aliquoted into Eppendorf tubes and stored at -80 ^{o}C for NMR studies.

Expression and Purification of Selectively ^{15}N-labeled Ala and Leu PchB

Expression and purification of selectively ^{15}N-labeled Ala and Leu PchB was performed as previously described[11] with modifications shown above. The minimal media was supplemented with 250 mg of the labeled amino acid per one liter growth with an additional 900 mg of unlabeled Val, Leu, Gly and Ile for ^{15}N-labeled Ala growths with Val and Ile for ^{15}N-labeled Leu growths.

NMR Spectroscopy

NMR data were acquired at room temperature (25 ^{o}C) on a Bruker Avance 800 MHz spectrometer and was processed and analyzed using NMRPipe[12] and NMRView[13]. A uniformly ^{13}C-^{15}N labeled PchB mutant K42H protein sample at a 2.0 mM concentration was used to collect the following 3D data sets: HNCA[9], CBCA(CO)NH[9] HNCACB.[10] Resonance assignments were determined by 2D ^{1}H-^{15}N HSQC experiments at various concentrations between 0.3 mM and 1.5 mM for ^{15}N Ala and ^{15}N Leu selectively[11] labeled PchB mutant K42E and uniformly labeled ^{15}N PchB mutant K42H along with previously mentioned 3D data sets. Flip-back pulses and pulsed field gradients were used to achieve water suppression.

Optimization of NMR Buffers

Preparation of NMR Samples

The preparation of NMR samples consisted of protein concentration using ultra centrifugal devices (Amicon, 3K NMWL) until ~two milliliters of concentrated PchB was achieved. The buffer system was swapped with an NMR suitable buffer using a PD-10 desalting column (GE Healthcare) using the spin protocol to prevent any substantial loss. The resultant protein sample was concentrated again using ultra centrifugal devices (Amicon, 3K NMWL) until a volume of 500 uL was achieved. The protein concentration was determined by UV absorbance at 280 nm after treatment with 6M guanidine-HCl. The sample was transferred to an eight inch NMR tube (Kontes) suitable for use in an 800 MHz spectrometer. Samples that showed good HSQC results were hermetically sealed to prevent contamination and stored at 4 ^{O}C for use in future NMR studies.

Phosphate-NaCl Buffer Conditions

The original buffer conditions for PchB NMR samples consisted of 20 mM phosphate, 20 mM NaCl and 10% D_2O (pH=7). The pH of the buffer system was determined by combining equal molar concentrations of mono and di-basic phosphate solution until the desired pH was reached. Samples were originally found to be stable after 24 hours. However, these same samples began to show signs of precipitation (white & cloudy) at 36 hours with increasing precipitation as at time went on. This resulted in a decreased NMR signal and poor HSQC spectra. Optimization steps were taken to increase solubility of PchB with progressively high NaCl concentrations (50 mM, 75mM). The changes in NaCl concentration yielded stabilization in the short term (24-48 hours) but ultimately resulted in a delayed precipitation effect similar to

the original buffer conditions with precipitation persistently increasing over time and found to be unsuitable for consistency among long term and future NMR studies.

Deuterated Tris Buffer Conditions

To increase the solubility of PchB in an NMR suitable buffer, deuterated Tris (50 mM) and NaCl (75-100mM) were incorporated. The new NMR buffer consisted of deuterated 50 mM Tris pH=7,100 mM NaCl and 10% D_2O. The pH of the buffer system was determined by titration with concentrated HCl (12 N) until the desired pH of 7.5 was reached. This new buffer condition resulted in highly soluble PchB with no protein precipitation over time. It should be noted that this buffer system is closely related to the buffer system used during the final stage of non-labeled PchB purification (50 mM Tris- pH=8, 150 mM NaCl, 10% glycerol). The resultant protein sample showed an improved HSQC over the original NMR buffer conditions and was subsequently used for collection of 3D data sets.

3.3 Results

The PchB mutant K42H was used in this NMR analysis. Analysis of the CBCA(CO)NH and HNCA data sets resulted in 32 out of the 101 amino acids assigned (Figure 3-2). The method of analysis for resonance assignments was dependent on the HNCA and CBCA(CO)NH data sets. The process of assignment in NMR analysis is dependent on correlating protons through other spin systems (^{13}C, ^{15}N) or through other protons in what is known as through-bond relationships.[14] Protons produce what is referred to as a chemical shift position which can be thought of as a peak dependent on the specific environment experienced within the protein. This idea is illustrated in Figure 3-3 where each peak can be thought of as having a unique ^{1}H and ^{15}N chemical shift resulting in a 2D map of each specific backbone proton seen through the bond of

Figure 3-2. Assigned ^{1}H-^{15}N HSQC Spectra of PchB K42H. Full view of the ^{1}H-^{15}N HSQC spectra for the PchB mutant K42H at pH=7. The assigned peaks below represent 32 out of the 101 amino acids of PchB.

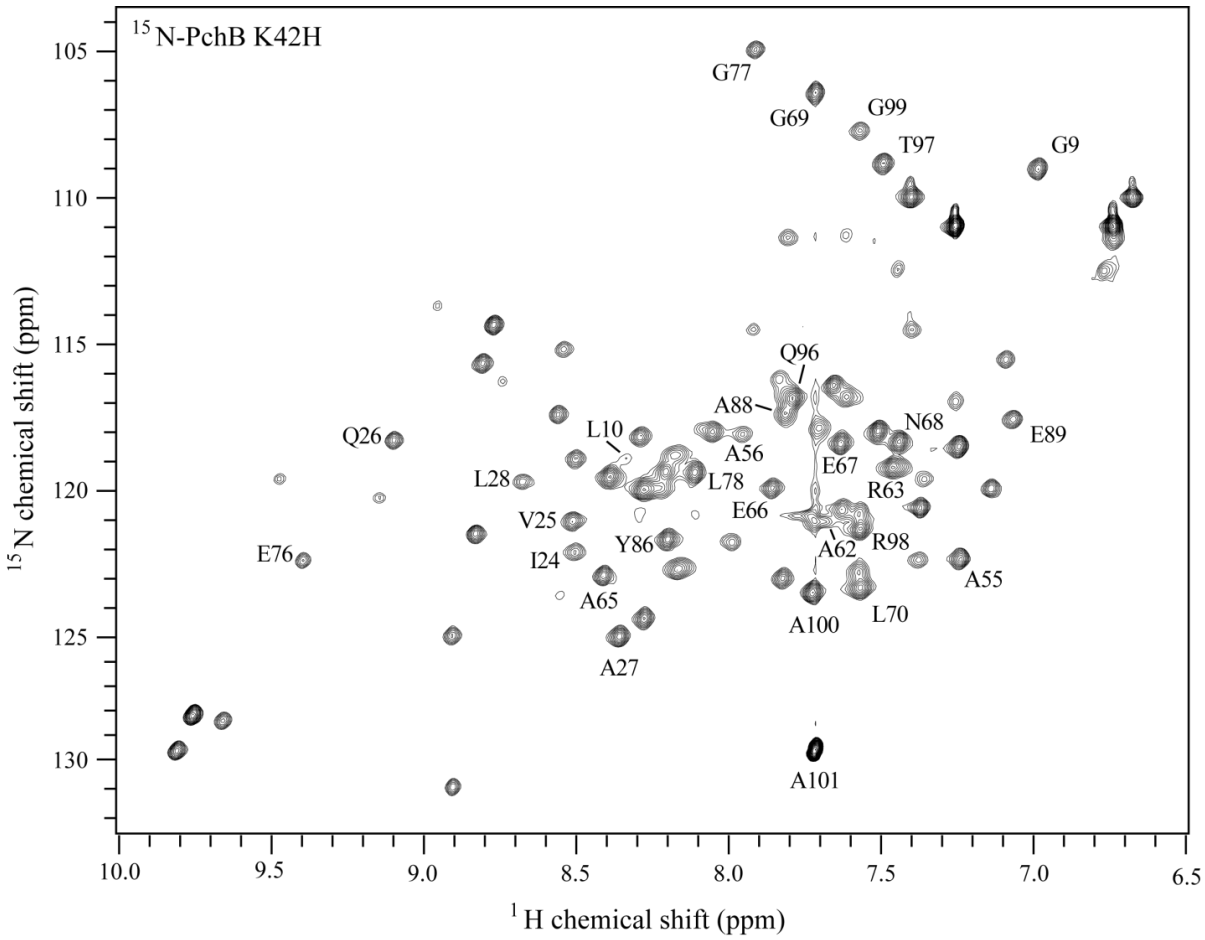

Figure 3-3. ^{1}H-^{13}C HNCA Spectra of PchB K42H. A set of ten assigned sequential amino acids are shown below with specific designations shown at the top of the strips. Notice the G69 which has a very characteristic α-carbon (^{13}C) chemical shift ~45 ppm which was used as a starting point in assignment. The resultant strips show the matching of the α-carbon (^{13}C) shifts and sequential "stair-stepping" used in backbone resonance assignment.

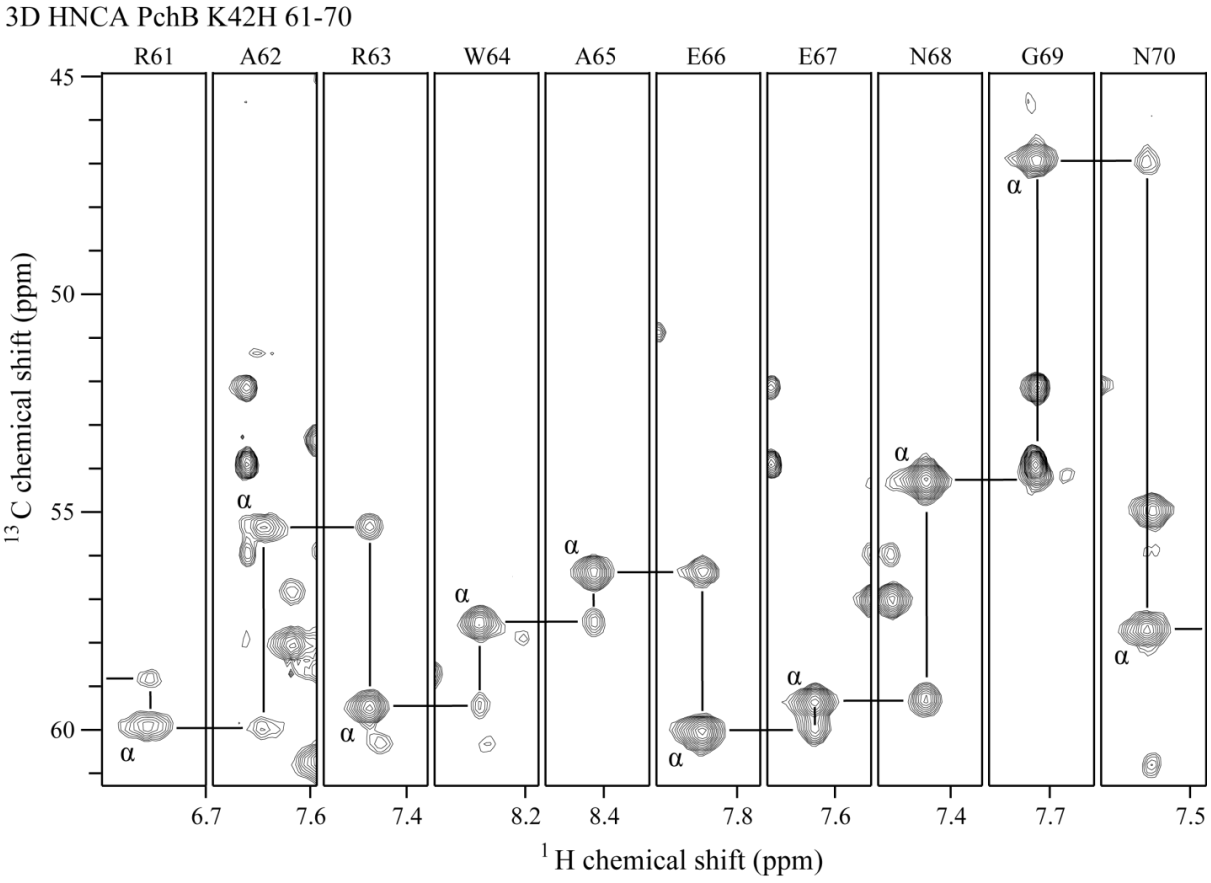

an attached ^{15}N in PchB.[14] In essence the HSQC shown in Figure 3-2 is representative of each amino acid within PchB. The challenge is assigning each specific peak in the HSQC to a specific amino acid in the sequence of PchB, which in our case is aided by the use of another spin system (^{13}C) and further experiments.

The HNCA experiment is used for assignments by its ability to correlate the chemical shifts of the α-carbon (^{13}C) of the current amino acid (*n*, strong peak) and the α-carbon (^{13}C) of the previous peak (*n*-1, usually weaker peak). Since the magnetism originates at the amide bond of a specific amino acid and is then sequentially transferred through J coupling (through-bond) to the α-carbons of the current and previous amino acid the two resultant peaks will share the same ^{1}H and ^{15}N chemical shifts but exhibit a different ^{13}C chemical shift^{N} as seen in the *individual* strips in Figure 3-3. Since all amides in the protein are excited at once, these two unique peak signals are also produced for every single α-carbon (^{13}C) amino in the protein, resulting in a strong and weak peak that share the same ^{13}C chemical shift but with different ^{1}H chemical shifts, which are the result of "seeing" the α-carbon through its amide bond (*n*, strong peak) and the amide bond of the next amino acid (*n*+1, weak peak) as seen in the *adjacent* strips in Figure 3-3.[14] This results in every amino acid being able to "see" the previous amino acid (*n-1)* while at the same time being "seen" by the following amino acid (*n*+1). These chemical shifts peaks can then be used to correlate the ^{13}C α-carbons and piece together the backbone resonances resulting in assigning the individual peaks shown in the HSQC with a specific amino acid (Figure 3-2).[14]

Confirmation of the assignments made through HNCA data analysis was performed through the CACB(CO)NH experiment. Analysis of this experiment yields two peaks representative of the α and ß-carbons (^{13}C) of the preceding residue in the peptide sequence each with a differing ^{13}C chemical shift as shown in the individual strips in Figure 3-4.[14] The α and ß-

carbons (^{13}C) shifts are correlated to a range of expected values recorded for the individual twenty amino acids thereby supporting or ruling out "matching" strips in the HNCA.

The process of assignment can also be aided in through selective labeling of individual amino acids.[11] As mentioned previously labeling results in HSQC peaks representative of the specific labeled amino acids chosen. This can be very helpful in identifying the nature of peaks that are difficult to assign otherwise but only serves to narrow down the possible peaks out of the total number of peaks. Take for example the results for ^{15}N-labeled alanine (green) and ^{15}N-labeled leucine (red) as shown in Figure 3-5. PchB contains a total of 18 alanine and six leucine residues which closely match the number of peaks shown for each respective HSQC. While the selectively labeled approach narrows down the field by identifying the alanine or leucine peaks within a spectra it still does not result in specific assignments and as such must be used in conjunction with data from other experiments such as the HNCA.

Figure 3-4. ^{1}H-^{13}C CACB(CO)NH Spectra of PchB K42H. A set of nine assigned (R61-G69) and one yet to be assigned (E60) sequential amino acids are shown below with specific designations shown at the top of the strips. Each strip is representative of the (*n*-1) ^{13}C-α and ß carbons. Notice the G69 which has a very characteristic α-carbon (^{13}C) chemical shift ~45 ppm and other strips which was used to check assignments made through the HNCA.

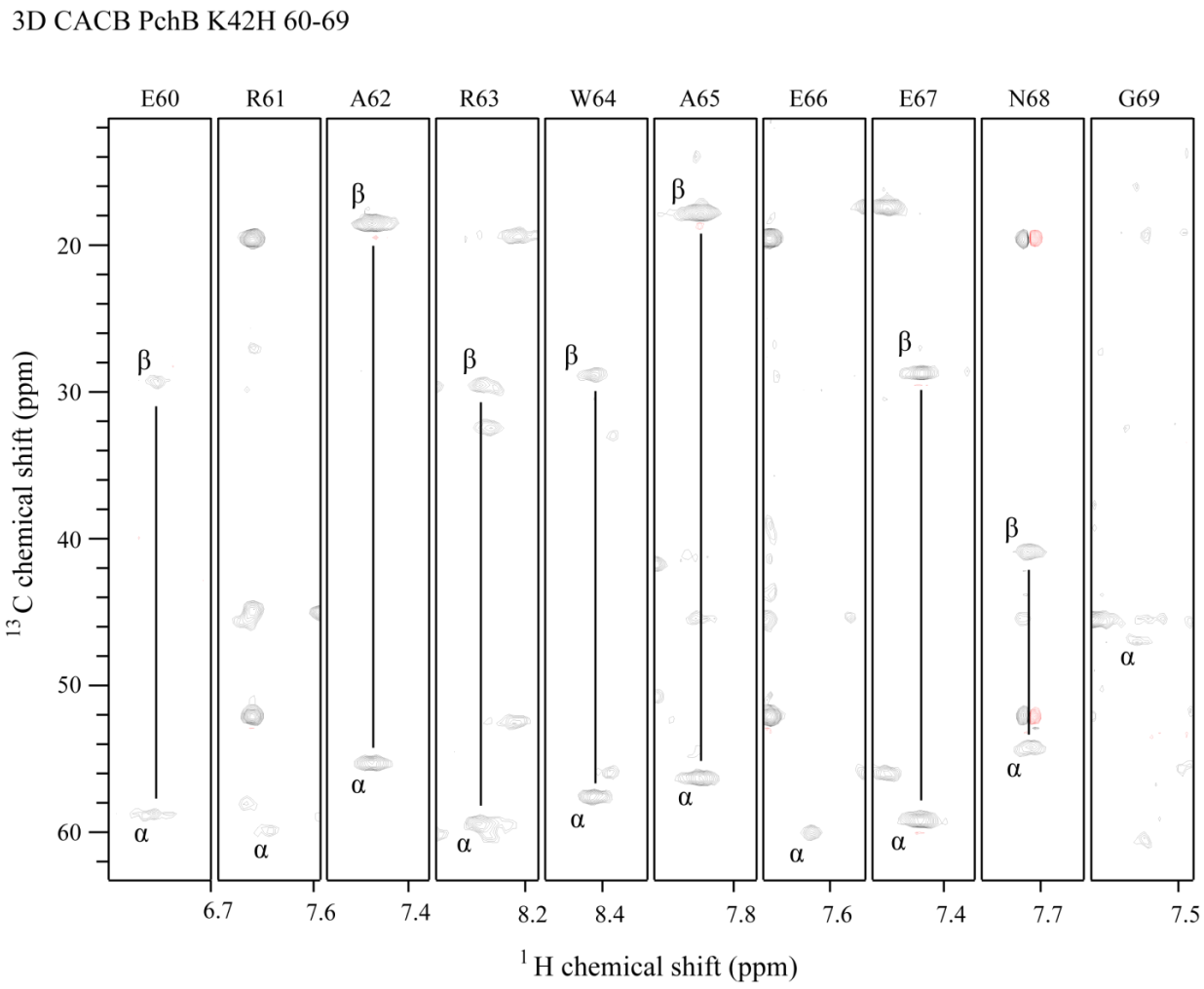

Figure 3-5. ^{1}H-^{15}N HSQC Spectra of PchB K42H with ^{15}N-labeled Ala and Leu Overlays. Full view of the ^{1}H-^{15}N HSQC spectra for the PchB mutant K42H at pH=7. The green peaks are representative of the ^{1}H-^{15}N alanine HSQC of PchB K42E. Notice ~15 peaks are visible out of the total 18 within the protein. The red peaks are representative of the ^{1}H-^{15}N leucine HSQC of PchB K42E. Notice that five peaks are visible out of a total of five leucine within PchB.

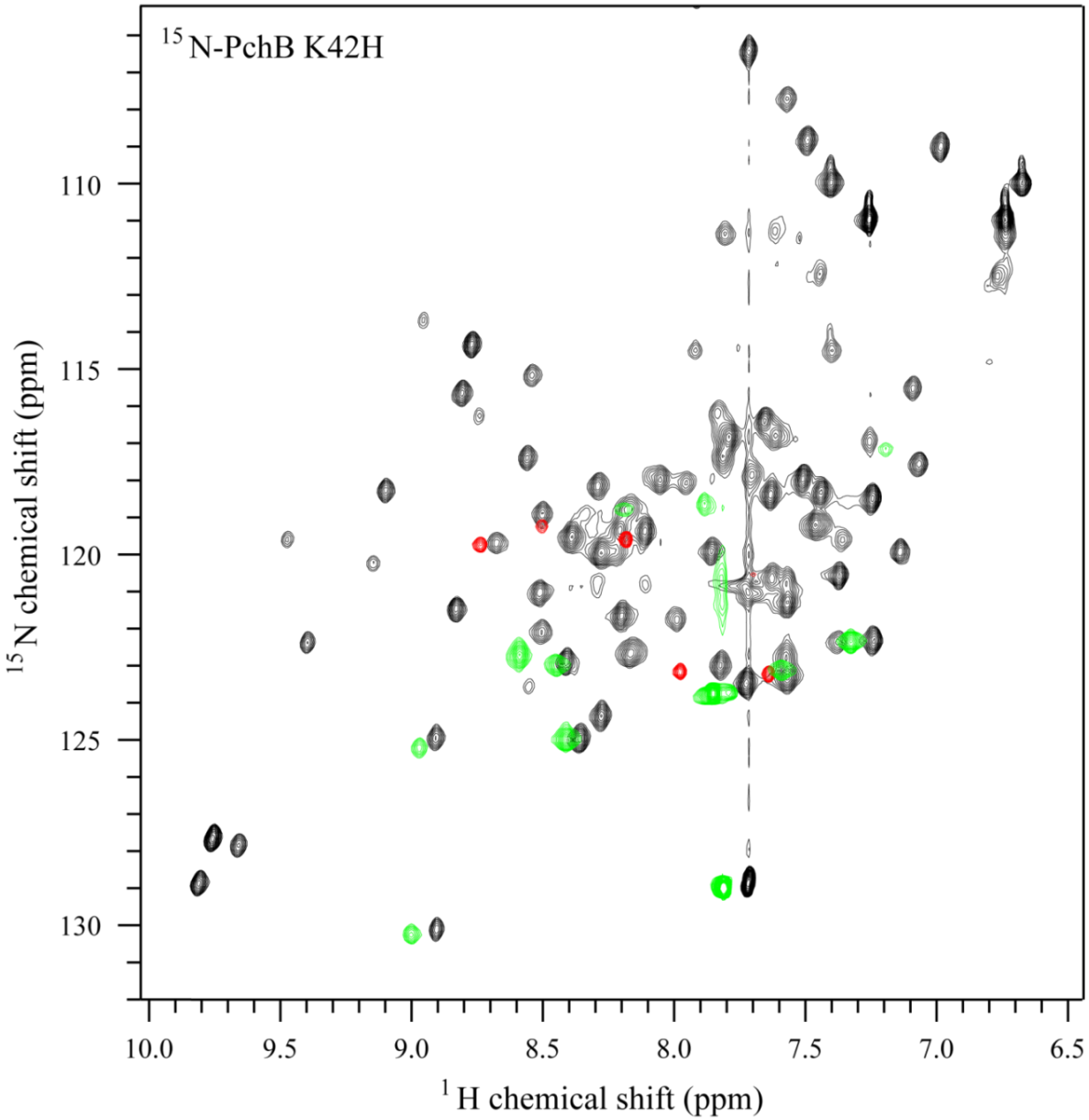

3.4 Discussion

Through the use of NMR spectroscopy, protein dynamics can be studied by looking at the relaxation rates of individual nuclei within a given protein.[14,15] These relaxation rates are used to correlate the overall flexibility of the protein through the summation of the flexibility of individual amino acids.[14] This information can be used to correlate structural dynamics to aspects of protein function such as contributions to catalytic activity.[15]

Before relaxation data can be utilized the backbone resonance assignments must first be made for the regions of interest. While the PchB mutant K42H was chosen as the main foundation for this thesis, initially selectively labeled ^{15}N-alanine and ^{15}N-leucine K42E were generated to aid in the backbone resonance assignments of previously collected NMR data for the PchB mutant K42E and were used to aid in the assignment of PchB mutant K42H (Figure 3-5). The PchB mutant K42H was chosen due its unique titratable IPL and CM activity[4] and also for the potential of future structure determination. The majority of peaks shown in the PchB mutant K42H HSQC in Figure 3-2 are associated with backbone resonances of the individual amino acids in PchB. The peaks can then be assigned to a particular amino acid based on chemical shift data (Figure 3-3, 3-4). Currently out of the 101 amino acids in PchB mutant K42H 32 backbone resonances have been assigned (Figure 3-2). All of the current assignments have been made in areas away from the active site loop region (light blue, Figure 3-6). Future work is needed to complete the backbone resonance assignments. Once all of the backbone resonance assignments have been made they can be used to evaluate relaxation data that provides structural dynamic information for individual amino acids and also the flexibility of the overall structure.

Figure 3-6. Secondary Structure of PchB. The highly alpha-helical secondary structure of a single monomer of PchB mutant K42H is shown below as cylinders with corresponding sequence alignment. The areas highlighted in blue represent the current backbone resonance assignments. The area highlighted in red represent the active site loop region with * showing the K42H mutation.

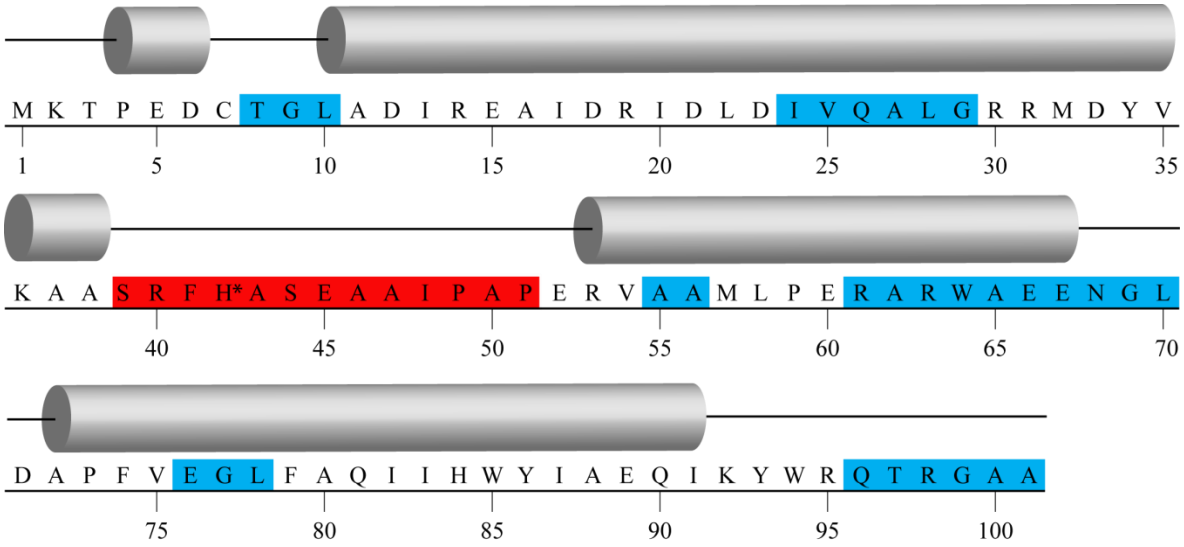

This information can then be used to correlate the active site loop dynamics and characterize its contribution to catalytic activity in PchB.

In the case of PchB, the relaxation data (T_1, T_2, hetNOE) can be used to correlate the active site loop dynamics and contribution to catalysis.[15,16] For the active site loop dynamics to play a role in the catalysis, the motions of the active site loop must first occur on a time scale relevant to catalysis. The k_{cat} for the IPL activity of the PchB mutant K42H is ~0.037 s^{-1} [3]. In other words, one molecule of isochorismate is converted to salicylate and pyruvate every 27 seconds (WT PchB = 6 seconds). This is not to say that only one molecule of isochorismate binds within the active site and then proceeds to take 27 seconds to surmount the transition state. However only once every 27 seconds does the combined effort of initial binding, electrostatics, loop dynamics and molecular breathing, result in a catalytic event. NMR relaxation measurements will be able to probe the timescale of the active site loop dynamics while also providing information on the flexibility of the macromolecule. Future NMR analysis will be able to elucidate and assess the contribution of PchB's active site loop dynamics towards IPL and CM activity.

References

1. Karplus, M. Molecular dynamics simulations of biomolecules. *Acc Chem Res* **35**, 321-323 (2002).
2. Schramm, V.L. Enzymatic transition states and transition state analog design. *Annu Rev Biochem* **67**, 693-720 (1998).
3. Mader, M.M. & Bartlett, P.A. Binding Energy and Catalysis: The Implications for Transition-State Analogs and Catalytic Antibodies. *Chem Rev* **97**, 1281-1302 (1997).
4. Lou, Q., Oulcha, J. & Lamb, A.L. Structure-function analyses of isochorismate-pyruvate lyase from *Pseudomonas aeruginosa* suggest differing catalytic mechanisms for the two pericyclic reactions of this bifunctional enzyme. *J Biol Chem* **48**, 5239-5245 (2009).
5. Zaitseva, J., Lu, J., Olechoski, K.L. & Lamb, A.L. Two crystal structures of the isochorismate pyruvate lyase from *Pseudomonas aeruginosa*. *J Biol Chem* **281**, 33441-33449 (2006).
6. Dernth, J. X-ray Diffraction: Princples. *eLS*. 2003.
7. Dundas, J., et al. CASTp: computed atas of surface topography of proteins with structural and topographical mapping of functionally annotated residues. *Nucl Acids Res* **34**, 116-118 (2006).
8. Grzesiek, S. & Bax, A. The importance of not saturating H2O in protein NMR. Application to sensitivity enhancement and NOE measurements. *J Am Chem Soc* **115**, 12593–12594 (1993).
9. Grzesiek, S., Dobeli, H., Gentz, R., Garotta, G., Labhardt, A. M. & Bax, A. 1H, 13C, and 15N NMR backbone assignments and secondary structure of human interferon-gamma. *Biochemistry* **31**, 8180–8190 (1992).
10. Wittekind, M. & Mueller, L. (1993). HNCACB, a high sensitivity 3D NMR experiment to correlate amide proton and nitrogen resonances with the α-carbon and β-carbon resonances in proteins. *J Magn Reson* **101**, 201–205 (1993).
11. Dahlquist, W., et al. Proton NMR Measurements of Bacteriophage T4 Lysozyme Aided by 15N Isotopic Labeling: Structural and Dynamic Studies of Larger Proteins. *PNAS* **84**, 1244-1248 (1987).
12. Delaglio F., et al. NMRPipe: a multidimensional spectral processing system based on UNIX pipes. *J Biomol NMR* **6**, 277–293 (1995).
13. Johnson BA., Using NMRView to visualize and analyze the NMR spectra of macromolecules. *Methods Mol Biol* **278**, 313–352 (2004).
14. Jacobsen, N., NMR Spectroscopy Explained (Wiley, 2007).
15. Kay, L., Torchia, D., & Bax, A. Backbone Dynamics of Proteins As Studied by ^{15}N Inverse Detected Heteronuclear NMR Spectroscopy: Application to Staphylococcal Nuclease. *Biochemistry* **28**, 8972-8979 (1989).
16. Flemming, H., &Vallurupalli, P. Using relaxation dispersion NMR spectroscopy to determine structures of excited, invisible protein states. *J Biomol NMR* **41**, 113-120 (2008).

CHAPTER 4

Conclusion

Enzymes act as catalysts for chemical reactions in all biological systems. Some enzymes exhibit enhancement rates of 10^{20} that produce products with every encounter within solution.[1,2,3] The catalytic mechanisms that drive these reactions can be as fundamental as the initial binding interactions between enzyme and substrate or can include a consortium of specialized catalytic mechanisms such as general acid-base, covalent intermediates, metal ions and proximity effects to lower the activation energy of a reaction and stabilize the transition state.[4,5] The major goal of this thesis is elucidating the fundamental forces that drive catalysis in PchB. Implications for this work include advancing fundamental theories of enzyme catalysis and also the rational drug design of novel antibiotics based on our understanding of these fundamental forces. These are age old pursuits in the field of enzymology answered through the ideas of transition state theory[6,7] and reactive substrate destabilization[8] each striving to explain the forces behind enzyme catalysis from different viewpoints.

This thesis focuses on answering these questions through structural and dynamic studies of PchB , an isochorismate pyruvate-lyase (IPL) from *Pseudomonas aeruginosa* that shows adventitious activity as a chorismate mutase (CM).[9] There has been significant work done involving chorismate mutases, of which PchB is a structural homologue, in understanding the fundamental forces that drive catalysis and the pericyclic reactions they catalize.[7,8,10-12] PchB is unique in biology in its ability to catalyze two pericyclic reactions within one active site.[9,13]

Pericyclic reactions are single substrate reactions that proceed through none of the classical mechanisms of general acid-base, covalent or metal ion catalysis and thus make an ideal system from which to elucidate the fundamental forces that drive enzyme catalysis.

Researchers that propose that transition state stabilization is responsible for activity within chorismate mutases argue that electrostatic stabilization of developing negative charge within the transition state intermediate is essential for activity.[7] This is in direct contrast to those that support a NAC[8] idea of catalysis where the enzyme constrains the substrate into what can be thought of as a reactive substrate conformation that can then proceed to the transition state without any further input from the enzyme. The structural and mechanistic studies within this thesis support a view that both of these theories contribute to the activity of PchB.

The structural and mutational mechanistic studies on residue 42 show that when a positive charge is present, such as in WT PchB with lysine 42, catalysis is most efficient.[13] The structural studies of WT PchB support the idea of transition state theory through placement of residue 42 in which the lysine supports the developing negative charge in the transition state intermediate. This idea of charge stabilization is also supported in the structural and mechanism studies of PchB mutant K42E.[13] When the positive charge of lysine is replaced with a negative charge in glutamic acid, no detectable IPL or CM activity is exhibited. The structural studies of K42E show that the active site architecture is conserved among both WT and PchB mutant K42E. This means that the placement of a negative charge in position 42 would not support a developing negative charge in the transition state intermediate, hindering passage to the transition state.

While there is structural evidence to support a positive charge for efficient catalysis, this does not mean that a positive charge is required for catalysis. The mutational and structural

studies of PchB mutant K42A support the idea of a NAC for PchB catalysis through the removal of any charge at position 42.[13] While a positive charge exhibits the most efficient catalysis, the removal of charge is still sufficient to promote catalysis. The active site architecture is conserved among the WT and PchB mutant K42A with the only major difference is that of the length of the side chain. While the K42A mutant is sufficient for catalysis the catalytic efficiency (k_{cat}/K_m) is 10^2 compared to 10^4 ($M^{-1}s^{-1}$) for WT PchB.[13] The activity of K42A is significantly less than that of WT PchB but K42A is still able to catalyze the reaction with a rate enhancement over that of the uncatalyzed reaction.

While our findings here support both the ideas of transition state theory and that of the NAC more questions arise in regards to the active site loop dynamics of PchB. If all of the active sites of the WT and PchB mutants have similar active site architectures and exhibit multiple orders of magnitude differences in activity what role does the active site loop dynamics play in catalysis? If the ability to bind the transition state is impaired relative to each PchB mutant but the active site architecture is maintained when the products of catalysis are bound in the active site, then there must be an event prior to product formation that differs among WT and PchB mutants. The answer likely has to do with the highly flexible active site loop region of PchB.[14] In this thesis the foundation of the Nuclear Magnetic Resonance (NMR) studies is laid out for further investigation. Further investigation into NMR relaxation rates of the active site loop is needed to fully elucidate the dynamics and the role of the active site loop in PchB catalysis.

The enormous rate enhancements that enzymes produce for chemical reactions are truly a summation of the fundamental forces that drive catalysis and a testament of the evolutionary processes that hone these forces. By breaking these forces down into their component vectors through targeted mutagenesis, selective co-crystallization and relaxation NMR studies we are

able to elucidate the fundamental forces that drive enzyme catalysis and make significant contributions to the field of enzymology as a whole.

References

1. Borman, S. Much ado about enzyme mechanisms. *C&E News* **88**, 35-39 (2004).
2. Wolfenden, R. & Snider, M.J. The depth of chemical time and the power of enzymes as catalysts. *Acc Chem Res* **34**, 938-945 (2001).
3. Alberty, R., Hammes, G., Application of the Theory of Diffusion-Controlled Reactions to Enzyme Kinetics. *J Phys Chem* **62**, 154-162 (1958).
4. Nelson, D.L. & Cox, M.M. Lehninger Principles of Biochemistry (2005).
5. Voet, D. & Voet, J.G. Biochemistry (Wiley, 2004).
6. Pauling, L. Nature of forces between large molecules of biological interest. *Nature* **161**, 707-709 (1948).
7. Warshel, A. et al. Electrostatic basis for enzyme catalysis. *Chem Rev* **106**, 3210-3235 (2006).
8. Bruice, T.C. & Lightstone, F.C. Ground state and transition state contributions to the rates of intramolecular and enzymatic reactions. *Acc Chem Res* **32**, 127-136 (1999).
9. Gaille, C., Kast, P. & Haas, D. Salicylate biosynthesis in *Pseudomonas aeruginosa*. Purification and characterization of PchB, a novel bifunctional enzyme displaying isochorismate pyruvate-lyase and chorismate mutase activities. *J Biol Chem* **277**, 21768-21775 (2002).
10. Liu, D.R., Cload, S.T., Pastor, R.M. & Schultz, P.G. Analysis of active site residues in *Escherichia coli* chorismate mutase by site-directed mutagenesis. *J Am Chem Soc* **118**, 1789-1790 (1996).
11. Hur, S. and Bruice, T. C. The mechanism of catalysis of the chorismate to prephenate reaction by the *Escherichia coli* mutase enzyme *Proc Natl Acad Sci U S A* **99**, 1176-1181 (2002).
12. Hur, S. and Bruice, T. C. The near attack conformation approach to the study of the chorismate to prephenate reaction *Proc Natl Acad Sci U S A* **100**, 12015- 12020 (2003).
13. Luo, Q., Olucha, J. & Lamb, A.L. Structure-Function Analyses of Isochorismate-Pyruvate Lyase from *Pseudomonas aeruginosa* Suggest Differeing Catalytic Mechanisms for the Two Pericyclic Reactions of This Bifunctional Enzyme. *Biochemistry* **48**, 5239-5245 (2009).
14. Zaitseva, J., Lu, J., Olechoski, K.L. & Lamb, A.L. Two crystal structures of the isochorismate pyruvate lyase from *Pseudomonas aeruginosa*. *J Biol Chem* **281**, 33441-33449 (2006).